



UNIVERSITY OF LEEDS

This is a repository copy of *Nature of the Cuvier Abyssal Plain crust, offshore NW Australia*.

White Rose Research Online URL for this paper:
<https://eprints.whiterose.ac.uk/171961/>

Version: Accepted Version

Article:

Reeve, MT, Magee, C orcid.org/0000-0001-9836-2365, Bastow, ID et al. (4 more authors) (2021) Nature of the Cuvier Abyssal Plain crust, offshore NW Australia. *Journal of the Geological Society*. ISSN 0016-7649

<https://doi.org/10.1144/jgs2020-172>

Reuse

Items deposited in White Rose Research Online are protected by copyright, with all rights reserved unless indicated otherwise. They may be downloaded and/or printed for private study, or other acts as permitted by national copyright laws. The publisher or other rights holders may allow further reproduction and re-use of the full text version. This is indicated by the licence information on the White Rose Research Online record for the item.

Takedown

If you consider content in White Rose Research Online to be in breach of UK law, please notify us by emailing eprints@whiterose.ac.uk including the URL of the record and the reason for the withdrawal request.



eprints@whiterose.ac.uk
<https://eprints.whiterose.ac.uk/>

1 Nature of the Cuvier Abyssal Plain crust, offshore NW Australia

2
3 Running title: Origin of the Cuvier Abyssal Plain

4
5 Matthew T. Reeve¹, Craig Magee^{1,2*}, Ian D. Bastow¹, Carl McDermott¹, Christopher A.-L.
6 Jackson^{1,4}, Rebecca E. Bell¹, Julie Prytulak³

7
8 ¹Basins Research Group (BRG), Department of Earth Science and Engineering, Royal School
9 of Mines, Prince Consort Road, Imperial College London, SW7 2BP, England, UK.

10 ²School of Earth and Environment, University of Leeds, Leeds, LS2 9JT, UK.

11 ³Department of Earth Sciences, University of Durham, DH1 3LE, UK

12 ⁴Department of Earth and Environmental Sciences, The University of Manchester,
13 Williamson Building, Oxford Road, Manchester, M13 9PL, UK

14
15 *Correspondence (c.magee@leeds.ac.uk)

16 17 **Abstract**

18 Magnetic stripes have long been assumed to be indicative of oceanic crust. However,
19 continental crust heavily intruded by magma can also record magnetic stripes. We re-evaluate
20 the nature of the Cuvier Abyssal Plain (CAP), offshore NW Australia, which hosts magnetic
21 stripes and has previously been defined as oceanic crust. We show chemical data from a
22 basalt within the CAP, previously described as an enriched MORB, could equally be
23 interpreted to contain evidence of contamination by continental material. We also recognise
24 seaward-dipping reflector (SDR) sequences in seismic reflection data across the CAP.
25 Borehole data from overlying sedimentary rocks suggests these SDRs were emplaced in a

26 shallow-water (<200 m depths) or sub-aerial environment. Our results indicate the CAP may
27 not be unambiguous oceanic crust, but may instead comprise a spectrum of heavily intruded
28 continental crust through to fully oceanic crust. If the CAP represents such a continent-ocean
29 transition zone, adjacent unambiguous oceanic crust would be located >500 km further
30 offshore NW Australia than currently thought; this would impact plate tectonic
31 reconstructions, as well as heat flow and basin modelling studies. Our work also supports the
32 growing consensus that magnetic stripes cannot, by themselves, be used to determine crustal
33 affinity.

34

35 Supplementary material: Enlarged and uninterpreted versions of the magnetic data and
36 seismic reflection lines are available at.

37

38 The discovery of magnetic reversal anomalies (stripes) across oceanic basins was
39 fundamental to the development of plate tectonic theory (e.g., Vine & Matthews 1963). These
40 magnetic anomalies arise from the interaction between the present-day magnetic field and
41 remanent magnetizations, records of past magnetic field polarity, acquired by igneous rocks
42 during their emplacement and crystallisation at contemporaneous seafloor spreading ridges
43 (Tivey et al. 1998). Where magnetic stripes occur adjacent to passive continental margins,
44 they are thus commonly interpreted to mark a basin's oldest, unambiguous oceanic crust
45 (e.g., Talwani & Eldholm 1973; Rabinowitz & LaBrecque 1979; Veevers 1986). However,
46 the progressive intrusion of magma into continental crust during break-up often leads to the
47 development of broad, complex zones whose structural and geochemical character can
48 display both a continental and oceanic affinity (e.g., Skogseid et al. 1992; Symonds et al.
49 1998; Planke et al. 2000; Skogseid et al. 2000; Direen et al. 2007; Bastow & Keir 2011;
50 Nirrengarten et al. 2020). Linear magnetic stripes akin to those hosted by unambiguous

51 oceanic crust have been identified within COTZs such as: (i) the onshore Red Sea Rift in
52 Afar, Ethiopia where continental crust is heavily intruded (Bridges et al. 2012); (ii) along the
53 magma-poor passive margins offshore Iberia and Newfoundland, where magnetic anomalies
54 are recorded by magmatic intrusions emplaced into exhumed and serpentinitised mantle prior
55 to break-up (Bronner et al. 2011); (iii) across part of the magma-rich passive margin offshore
56 NW Australia (i.e. the Gascoyne margin; Direen et al. 2008); and (iv) offshore South
57 America where the margin comprises so-called ‘magmatic crust’ wholly consisting of new
58 igneous material, which differs from normal oceanic crust in that it formed via extension in a
59 sub-aerial and/or shallow-water setting, and not true deep-marine spreading (Collier et al.
60 2017; McDermott et al. 2018).

61 Given recent studies have shown magnetic stripes may not be diagnostic of oceanic
62 crust (e.g., Direen et al. 2008; Bridges et al. 2012; Collier et al. 2017; McDermott et al.
63 2018), it is worth re-evaluating the nature of areas previously defined as oceanic crust
64 adjacent to passive margins (Eagles et al. 2015; Causer et al. 2020). For example, the Cuvier
65 Abyssal Plain (CAP), offshore NW Australia hosts well-developed magnetic stripes
66 distributed about inferred spreading centres and has been interpreted as unambiguous oceanic
67 crust that formed at a half-spreading rate of $\sim 3.5\text{--}4.5\text{ cm yr}^{-1}$ (Fig. 1) (e.g., Falvey & Veevers
68 1974; Larson et al. 1979; Robb et al. 2005; Gibbons et al. 2012; MacLeod et al. 2017). Here,
69 we investigate the origin of the CAP, offshore NW Australia through an integrated analysis
70 of 2D seismic reflection data, magnetic data, and a re-examination of published chemical
71 data. We show packages of seaward-dipping reflector (SDR) sequences occur across the
72 CAP, occasionally spanning several magnetic stripes, and probably represent lavas emplaced
73 in sub-aerial or shallow-water conditions. We reinterpret chemical data from a basalt dredged
74 from an inferred spreading centre (the Sonne Ridge: Fig. 1A) and previously classified as
75 having an enriched MORB-like character (Dadd et al. 2015). However, due to sample

76 alteration this MORB-like interpretation is ambiguous and the basalt geochemistry could
77 equally be interpreted as having a component of continental contamination. Overall, our
78 observations question whether the CAP is unambiguous oceanic crust, and we suggest it
79 could instead comprise a spectrum of crustal types, ranging from heavily intruded continental
80 crust of the Cuvier Margin to fully magmatic crust generated in sub-aerial or shallow-water
81 environments. If our proposal that the CAP is COTZ is correct, the landward limit of
82 unambiguous oceanic crust adjacent to the Cuvier Margin may be located >500 km further
83 offshore: this would have implications for plate tectonic reconstructions involving the NW
84 Australian margin (cf. Heine & Müller 2005; Gibbons et al. 2012), as well as for heat flow
85 and basin modelling studies. More generally, our study supports previous suggestions that
86 magnetic stripes may not be a unique feature of oceanic crust.

87

88 **Continent-Ocean Transition Zone (COTZ) formation**

89 COTZs at magma-rich passive margins are typically characterised by seismically isotropic,
90 acoustically fast wavespeed ($>7 \text{ km s}^{-1}$) crust, overlain by SDR lava sequences emplaced
91 within sub-aerial or shallow-water environments (e.g., Eldholm et al. 1989; Larsen &
92 Saunders 1998; Symonds et al. 1998; Menzies et al. 2002). Observations from rifted margins
93 and active rifts suggest that these COTZs are marked by a compositional and structural
94 spectrum, bounded by unambiguous continental and oceanic crust end-members (Fig. 2).
95 From the landward limit of COTZs, we expect the proportion of magma intruded into
96 continental crust to increase oceanwards (Fig. 2) (e.g., Eldholm et al. 1989; Keranen et al.
97 2004; Daniels et al. 2014; Nirrengarten et al. 2020). As dyking localises, eventually no
98 continental crust will remain (i.e. break-up of continental crust), and the COTZ will solely
99 comprise igneous intrusions and extrusions emplaced along magmatic segments during sub-
100 aerial or shallow-water extension (Fig. 2) (e.g., Collier et al. 2017; Paton et al. 2017;

101 McDermott et al. 2018); this so-called new magmatic crust is similar to oceanic crust but
102 does not form by deep-marine spreading at a mid-ocean ridge and may be underlain by
103 continental lithospheric mantle (e.g., Bécel et al. 2020). Decay of the buoyant support of
104 these dense, sub-aerial or shallow-water magmatic segments will promote their subsidence
105 (e.g., Corti et al. 2015; McDermott et al. 2018). As these magmatic segments subside to water
106 depths of ≥ 2 km, plate-spreading drives the generation of unambiguous oceanic lithosphere,
107 the crust of which in magma-rich, fast-spreading areas (>4 cm yr⁻¹ spreading rates; Cannat et
108 al. 2019), like that characterising the CAP, is expected to comprise layers of pillow basalts,
109 sheeted dykes, and gabbro (e.g., McDermott et al. 2018). Across COTZs and into
110 unambiguous oceanic crust, we therefore expect an oceanwards reduction in the continental
111 signature of magma chemistry as they become more MORB-like (Fig. 2) (e.g., Nirrengarten
112 et al. 2020). Because of uncertainties in data resolution and interpretation, it is often difficult
113 to constrain the position from heavily intruded continental crust to the onset of magmatic
114 crust emplacement. We therefore combine these domains and refer to them both as a COTZ
115 (Fig. 2).

116

117 **Geological Setting**

118 *Crustal Structure and Age*

119 The ~400 km wide Gascoyne and 180 km-wide Cuvier margins, which are separated by the
120 NW-trending Cape Range Fracture Zone, form part of the NW Australian magma-rich
121 passive margin (Fig. 1A). This passive margin is bound by the Argo Abyssal Plain to the
122 north, and the Gascoyne Abyssal Plain and Cuvier Abyssal Plain (CAP) to the west (Fig. 1A)
123 (Longley et al. 2002; Stagg et al. 2004). Margin formation occurred during multiple phases of
124 Permian-to-Late Jurassic rifting, culminating in Early Cretaceous break-up of the Gascoyne
125 and Cuvier margin rift segments from Greater India (Fig. 3A) (Longley et al. 2002). A 200–

126 250 km wide COTZ (i.e. the Gallah Province) has been interpreted along the Gascoyne
127 Margin to consist of a seismically high-velocity lower crust, overlain by 2–5.5 km thick SDR
128 sequences, which overall record M-series magnetic anomalies M10N–M5n (~136–131 Ma,
129 Valanginian-to-Hauterivian; Figs 1A and B) (Symonds et al. 1998; Robb et al. 2005; Direen
130 et al. 2008; Rey et al. 2008); some recent studies have assumed the Gallah Province
131 comprises oceanic crust but have not justified why a COTZ origin is dismissed (e.g., Fig. 1C)
132 (e.g., Gibbons et al. 2012). If the Gallah Province is a COTZ and thus marks the final stages
133 of continental break-up and, the identification of magnetic chron M3n within unambiguous
134 oceanic crust of the adjacent Gascoyne Abyssal Plain indicates that full continental
135 lithospheric rupture and oceanic seafloor spreading occurred by ~130 Ma (Hauterivian; Figs
136 1B and 3A) (Robb et al. 2005; Direen et al. 2008). Along the Cuvier Margin, beneath the
137 modern continental slope, seismically imaged SDR sequences have previously been
138 interpreted to mark a COTZ, albeit only 50–70 km wide (e.g., Figs 1A and D) (Hopper et al.
139 1992; Symonds et al. 1998). Based on recognition of at least magnetic chron at least M10N–
140 M10 within the adjacent CAP it has been classified as oceanic crust that started forming at
141 ~136–134 Ma (Valanginian; Figs 1B and 3A) (e.g., Falvey & Veevers 1974; Larson et al.
142 1979; Robb et al. 2005; Gibbons et al. 2012). If the CAP comprises oceanic crust, these age
143 constraints on its formation suggest full continental lithospheric rupture of the Cuvier Margin
144 occurred ~4–6 Myr before the Gascoyne Margin (Fig. 3A).

145

146 *Cuvier Abyssal Plain structure, magnetics, and chemistry*

147 The CAP lies ~5 km below sea level and comprises a ~6–10.5 km thick crystalline crust (e.g.,
148 Fig. 1D) (Hopper et al., 1992). The CAP is bound to the SW by the Wallaby Plateau and
149 Wallaby Saddle, and within the CAP are two linear, NE-trending bathymetric highs that are
150 co-located with linear magnetic anomalies: the Sonne Ridge and Sonja Ridge (Figs 1A and

151 B). Robb et al. (2005) interpreted the magnetic anomalies southeast of the Sonne Ridge as
152 M10N–M6 (135.9–131.7 Ma) and conjugate to a more poorly developed set of anomalies
153 northwest of the ridge (Fig. 1B). These magnetic anomalies to the NW of the Sonne Ridge,
154 which terminate against the Cape Range Fracture Zone, are cross-cut by at least chron M5n?
155 (131.7–130.6 Ma) either side of the Sonja Ridge (Fig. 1B) (Robb et al. 2005). Based on
156 mapping of these chrons across the CAP, Robb et al. (2005) interpreted the Sonne and Sonja
157 ridges as oceanic spreading centres. Geochemical analyses of a basalt dredged from the
158 Sonne Ridge along its extension into the Wallaby Plateau, suggest it has a slightly enriched
159 MORB-like signature, supporting the inference that the Sonne Ridge is an oceanic spreading
160 centre (Dadd et al. 2015). An alternative interpretation forwarded for the Sonne Ridge is that
161 it represents a ‘pseudofault’ (i.e. an apparent offset in magnetic stripes formed by ridge
162 jumps; Hey 1977) separating oceanic crust to the SE from a north-eastern extension of the
163 ‘part-continental’ Wallaby Plateau (Fig. 1C); this interpretation is based on changes in
164 gravity intensity across the structure and the possible termination of the Cape Range Fracture
165 Zone directly north of the ridge (Gibbons et al. 2012). In their model, Gibbons et al. (2012)
166 define a different oceanic spreading centre, located ~100 km to the SE and parallel to the
167 Sonne Ridge, interpreted to be bordered by conjugate chrons M10–M8 (134.2–132.5 Ma)
168 (Fig. 1C). Gibbons et al. (2012) considered the Sonja Ridge to be an oceanic spreading
169 centre, which produced oceanic crust potentially recording chrons M7–M4, isolated within
170 the Wallaby Plateau (Fig. 1C). Beyond the CAP, chron M4 or M3n is the first to occur
171 continuously along-strike across both the Cuvier and Gascoyne margin segments (Figs 1B
172 and C).

173

174 *The Wallaby Plateau and Wallaby Saddle*

175 The Wallaby Plateau is a large bathymetric high (Figs 1A-C), containing up to ~7.5 km thick
176 sequences of volcanic and sedimentary rocks, which are typically expressed in seismic
177 reflection data as packages of diverging and dipping reflections that appear similar to SDRs
178 (e.g., Colwell et al. 1994; Daniell et al. 2009; Stilwell et al. 2012; Olierook et al. 2015).
179 Interpretation of seismic reflection and magnetic data, coupled with chemical,
180 geochronological, and biostratigraphic analyses of dredge samples, suggests the Wallaby
181 Plateau probably comprises ~124 Myr old, continental flood basalts and interbedded
182 sedimentary strata emplaced on a fragment of extended continental crust (see Olierook et al.
183 2015 and references therein). Between the Wallaby Plateau and the Australian continent is
184 the Wallaby Saddle, a bathymetric low containing SDRs but no magnetic stripes, interpreted
185 by Symonds et al. (1998) to comprise ‘transitional’ crust (i.e. non-oceanic; Figs 1A and B).
186 The Wallaby Plateau and Wallaby Saddle seemingly preserve a range of crustal types typical
187 of a COTZ, but not unambiguous continental crust or unambiguous oceanic crust.

188

189 *Sedimentary Cover on the Cuvier Abyssal Plain*

190 The top of the crystalline basement within the CAP corresponds to a high-amplitude
191 reflection in seismic data, which is overlain by a ~1–3.3 km thick, sedimentary succession
192 broadly comprising sub-horizontal reflections (e.g., Fig. 1D) (e.g., Veevers & Johnstone
193 1974; Hopper et al. 1992). Biostratigraphic and lithological data for the sedimentary cover
194 are available from the DSDP Site 263 borehole, which was drilled in 1972 and terminates
195 ~100–200 m above the basement (Figs 1A and 3B) (e.g., Bolli 1974; Scheibnerová 1974;
196 Wiseman & Williams 1974; Holbourn & Kaminski 1995). These data provide an important
197 record of subsidence history of the Cuvier Abyssal Plain. The lowermost 546 m of strata
198 penetrated by DSDP Site 263 comprise black claystones, which become silty and contain
199 abundant kaolinite towards the base of the borehole (Fig. 3B) (Robinson et al. 1974;

200 Compton et al. 1992). In places, particularly at the base of DSDP Site 263, these silty
201 claystones are poorly sorted and contain angular quartz grains (Robinson et al. 1974).
202 Analyses of benthic foraminifera from DSDP Site 263 suggest the black, kaolinitic claystones
203 are likely Hauterivian-to-Middle Barremian in age, passing upwards into Albian-to-Aptian
204 black claystones (Fig. 3B) (Holbourn & Kaminski 1995); these age ranges are supported by
205 dinoflagellate distributions and carbon isotope stratigraphy (Wiseman & Williams 1974;
206 Oosting et al. 2006). A gradual upwards transition from coarsely to finely agglutinated
207 foraminifera species, coupled with an upwards increase in the scarcity of shallow-water taxa
208 (e.g., *Hyperamina* spp.) and a corresponding decrease in grain size, suggests that the
209 Hauterivian-to-Middle Barremian strata record deepening neritic (i.e. <200 m water depth)
210 conditions (e.g., Fig. 3B) (Robinson et al. 1974; Veevers & Johnstone 1974; Holbourn &
211 Kaminski 1995; Oosting et al. 2006). Sedimentary rocks recovered from the Pendock-1
212 borehole, which is located on the Cuvier Margin continental shelf, are sedimentologically
213 similar and of comparable age to those penetrated in DSDP 263 (Veevers & Johnstone 1974;
214 Holbourn & Kaminski 1995). These similarities to Pendock-1 suggest that the Hauterivian-
215 to-Middle Barremian strata sampled by DSDP Site 263 can broadly be correlated to the
216 Winning Group of the North and South Carnarvon basins and likely do not contain products
217 of mass-wasting from the continental slope (Fig. 3) (Veevers & Johnstone 1974; Holbourn &
218 Kaminski 1995).

219

220 **Dataset and methodology**

221 *Seismic reflection data*

222 To assess the crustal structure of the CAP and surrounding areas, we interpret seven 2D
223 seismic lines from four, pre-stack time-migrated reflection surveys (Fig. 1A) (see
224 Supplementary Table 1 for acquisition and processing details for each survey). Seismic lines

225 EW0113-5, EW0113-6, and repro-n303 are each >400 km long and extend across parts of the
226 Cuvier Margin and the CAP; EW0113-5 and EW0113-6 span the mapped area of SDRs in the
227 Cuvier COTZ (Hopper et al. 1992) and the location of the extinct spreading centre proposed
228 by Gibbons et al., (2012), whereas repro-n303 images the Sonne Ridge (Fig. 1A). Due to
229 extreme amplitude contrasts between the shallow and deep sections of the original migrated,
230 EW0113 data, we applied a time-dependent gain filter and root filter to improve amplitude
231 balance and enhance deep reflectivity (see supplementary information for details). Lines
232 s135-05, s135-08, and s310-59 image the inferred ‘transitional’ crust of the Wallaby Saddle
233 and the intruded continental crust of the Wallaby Plateau (e.g., Symonds et al., 1998;
234 Goncharov and Nelson, 2012; Olierook et al., 2015). The NE-trending seismic line s135-11
235 was also interpreted as it ties together the margin-orthogonal seismic lines and provides a
236 margin-parallel image of the southernmost Exmouth Plateau continental crust, the CAP, and
237 the Wallaby Plateau (Fig. 1A).

238 Although time-migrated seismic reflection data allows us to qualitatively and
239 quantitatively characterise crustal structure, seismic velocity information is required to
240 convert depth information from seconds two-way time (TWT) to metres. To provide context
241 for the thicknesses and depths of some discussed structures, we depth-converted the
242 EW0113-5 and EW0113-6 seismic data using interval velocities derived from ocean-bottom
243 seismometer (OBS) data (Table 1) (Tischer 2006). The OBS array comprised 20 instruments
244 spaced ~16 km apart and was co-located with seismic line EW0113-6, which is situated ~70
245 km along-strike from line EW0113-5 (Fig. 1A); the geological structure imaged in line
246 EW0113-6 is very similar to that of EW0113-5, supporting the use of velocities from
247 EW0113-6 to depth convert both lines. As velocity data from across the Wallaby Plateau and
248 Wallaby Saddle is limited (Goncharov & Nelson 2012), and because along-strike variation in
249 geology will likely promote changes in the velocity structure, lines s135-05, s135-08, and

250 s310-59 are presented in time. For easier comparison between seismic data from the CAP and
251 the Wallaby Plateau and Wallaby Saddle, we do not depth-convert repro-n303 or s135-11.
252 Interpretation of reflection configurations (e.g., dip values) in time-migrated data are only
253 qualitative, and may change if depth-converted.

254

255 ***Magnetic data***

256 To examine the regional magnetic anomalies, we utilise the EMAG2v2 and EMAG2v3 Earth
257 Magnetic Anomaly Grids (Maus et al. 2009; Meyer et al. 2017). EMAG2v2 is a 2 arc min
258 resolution grid derived from marine, airborne, and satellite magnetic data, but uses *a priori*
259 information to interpolate magnetic anomalies in areas where data gaps are present (Fig. 4A)
260 (Maus et al. 2009; Meyer et al. 2017). In contrast, EMAG2v3 uses more data points to derive
261 magnetic anomaly maps but assumes no *a priori* information (Fig. 4B) (Meyer et al. 2017).
262 In ocean basins with a relatively poor coverage of magnetic data available, such as the CAP,
263 clear linear magnetic anomalies in EMAG2v2 thus typically appear poorly developed or are
264 absent in EMAG2v3 (cf. Figs 4A and B) (Meyer et al. 2017). This difference in the presence
265 and appearance of linear magnetic anomalies between grids is because (assumed) knowledge
266 of seafloor spreading processes was incorporated into, and therefore influenced, interpolation
267 during construction of the EMAG2v2 grid (Maus et al. 2009; Meyer et al. 2017). Importantly,
268 the apparent reduction in magnetic stripes observed in EMAG2v3, compared to EMAG2v2
269 (Figs 4A and B), does not necessarily mean these features are absent, but rather that the
270 available data is insufficient to unambiguously confirm their presence in non-directionally
271 gridded data such as EMAG2v3 (Meyer et al. 2017). Comparing the EMAG2v2 and
272 EMAG2v3 grids with shiptrack magnetic data (Robb et al. 2005) allows us to interrogate the
273 magnetic architecture of the CAP (cf. Meyer et al. 2017). In particular, we interpret the
274 EMAG2v2 data by picking the young end of the positive anomaly peaks (Fig. 1B), and

275 compare the defined anomalies to those observed in the EMAG2v3 grid and shiptrack
276 magnetic data. From these comparisons, we tied interpreted magnetic stripes to seismic line
277 EW0113-5, EW0113-6, and repro-n303 using the synthetic profiles of Robb et al. (2005). To
278 update the absolute ages of the interpreted magnetic anomalies (Robb et al. 2005), we use the
279 time-calibrated, magnetic polarity reversal sequence of Gradstein & Ogg (2012).

280

281 *Geochemical data*

282 To evaluate whether the Sonne Ridge is an extinct seafloor spreading centre (e.g., Mihut &
283 Müller 1998; Robb et al. 2005) consisting of oceanic crust with a MORB or MORB-like
284 affinity along its length, we examine chemical data from a dredged, altered basalt lava
285 sample collected along its extension into the Wallaby Plateau (i.e. Site 57 - sample
286 057DR051A; diamond 57 in Fig. 1A) (Daniell et al. 2009; Dadd et al. 2015; Olierook et al.
287 2015). We compare the Sonne Ridge sample to two samples collected from near the south-
288 western margin of the Wallaby Plateau (diamonds 55 and 52 in Fig. 1A) (i.e. Site 55 -
289 samples 055BS004A and 055BS004B) (Dadd et al. 2015). Two Wallaby Plateau basalts
290 dated from Site 52 (Fig 1A) yield plagioclase $^{40}\text{Ar}/^{39}\text{Ar}$ plateau ages of 125.12 ± 0.9 Ma and
291 123.80 ± 1.0 Ma, whereas two analyses of the Sonne Ridge sample yielded less precise ages of
292 120 ± 14 Ma and 123 ± 11 Ma (Olierook et al. 2015).

293

294 **Results**

295 *Reflection seismology*

296 *Cuvier Abyssal Plain*

297 We interpret a prominent, continuous, high-amplitude seismic reflection across the CAP; this
298 represents the interface between crystalline rock and overlying sedimentary strata (e.g., Figs
299 1D and 5). The Moho was picked at the base of a sub-horizontal zone of moderate-to-high-

300 amplitude, discontinuous seismic reflections, that coincides with a downwards increase in
301 seismic velocity from $\sim 7.2 \text{ km s}^{-1}$ to 8 km s^{-1} and is broadly flat-lying at $\sim 16\text{--}17 \text{ km}$ or $\sim 10 \text{ s}$
302 TWT (Fig. 5; Table 1). On EW0113-5, the Moho appears to become shallower oceanwards
303 (to depths $\leq 14 \text{ km}$), although our interpretation of repro-n303 suggests it may deepen again
304 beneath the Sonne Ridge (Figs 5A and D). Overall, the crystalline crust is $\sim 8\text{--}10 \text{ km}$ ($\sim 3\text{--}5 \text{ s}$
305 TWT) thick and is thickest at the Sonne Ridge where crystalline rock is elevated above the
306 adjacent sedimentary cover (Figs 1D and 5). In contrast to the appearance of the Sonne
307 Ridge, there is no evidence of crustal thickening or elevated basement where the spreading
308 ridge proposed by Gibbons et al., (2012) is expected on lines EW0113-5 and EW0113-6
309 (Figs 1A, C, and 5).

310 From our seismic reflection data we sub-divide the CAP crust into three distinct
311 seismic facies (Figs 5-8). Across the CAP, the $\sim 1\text{--}3 \text{ km}$ -thick, uppermost crystalline crustal
312 layer comprises a layered, moderate- to high-amplitude seismic facies (SF1; Fig. 5). On NW-
313 trending seismic lines orthogonal to the margin (i.e. EW0113-5, EW0113-6, and repro-n303),
314 SF1 locally contains $\leq 40 \text{ km}$ wide, $\leq 4.5 \text{ km}$ thick wedges of coherent, high-amplitude,
315 dipping reflections that predominantly diverge seaward (Figs 5 and 6); adjacent to the Sonne
316 Ridge on its NW side, a package of dipping reflections diverge landwards (Fig. 5D). There is
317 no correlation between the location and width of these wedges relative to the magnetic
318 chrons; e.g., some packages of seaward-diverging reflections span several chrons (Fig. 5).
319 Where well-developed wedges are absent, SF1 contains discontinuous, horizontal to gently
320 seaward-dipping reflections (Fig. 5). On line s135-11, which is oriented parallel to the
321 margin, most reflections within SF1 are either sub-horizontal or dip gently north-eastwards
322 (Fig. 7). Seismic velocities for SF1 are estimated to be $\sim 4\text{--}5 \text{ km/s}$ (Fig. 5; Tischer 2006).

323 In places, the uppermost crystalline layer (SF1) is underlain by a low-amplitude, near
324 transparent seismic facies (i.e. SF2), which is particularly clear on lines EW0113-5 and

325 EW0113-6 (Figs 5 and 6). SF2 is up to ~2.8 km thick, being thinnest and occasionally absent
326 beneath wedges of dipping reflections within SF1 (Figs 5 and 6). The few reflections that
327 occur within SF2 typically have low-to-moderate to amplitudes and variable dips (Figs 5 and
328 6). On repro-n303, at the seaward termination of an overlying wedge in SF1, a ~15 km wide
329 swarm of landward-dipping reflections are present in SF2 (Fig. 5D). There is no clear SF2
330 observed on line s135-11, even in areas where it is encountered on the intersecting margin-
331 orthogonal lines (Fig. 7).

332 Beneath SF2 we recognise a ~3.5–6 km (<2 s TWT) thick, low-amplitude layer that
333 locally contains prominent, high-amplitude, dipping reflections and discontinuous, moderate
334 amplitude, sub-horizontal reflections (SF3; Figs 5–7). On line EW0113-5, the inclined
335 reflections within SF3 terminate at the Moho and primarily dip oceanwards at 20–30° (Fig.
336 5A). On lines EW0113-6 and repro-n303, however, reflections within SF3 dip both
337 oceanwards and landwards (Figs 5B, C, and 6). Mapped reflections within SF3 on s135-11
338 primarily dip towards the SE, extending from the top of the layer down into the mantle,
339 cross-cutting but not offsetting NE-dipping, gently inclined reflections (Fig. 7). Similar mid-
340 and lower-crustal reflection configurations to SF2 and SF3, respectively, occur in the seismic
341 data presented by Hopper et al. (1992) (Fig. 1D). Seismic velocities of SF2 and SF3 are 6.8–
342 7.2 km/s (Fig. 4; Tischer 2006).

343

344 *Wallaby Plateau and Wallaby Saddle*

345 Building on previous investigations of seismic data across the continental-to-COTZ crust of
346 the Wallaby Plateau and Wallaby Saddle, here we (re)interpret several 2D seismic lines and
347 compare their structure to that of the CAP. Similar to the CAP, a prominent, continuous,
348 high-amplitude seismic reflection marks the interface between crystalline rock and overlying
349 sedimentary strata across the Wallaby Plateau and Wallaby Saddle (Figs 7 and 8). Within the

350 Wallaby Saddle, the crust appears to be ~5–6 s TWT thick, although the Moho can only
351 tentatively be interpreted, and can also be sub-divided into: (i) SF1, itself containing up to ~4
352 s TWT thick, 12 km wide wedges of diverging reflections that typically dip seawards; (ii)
353 restricted zones that are broadly transparent, with some low-to-moderate to amplitude
354 reflections with variable dips, similar to SF2 described from the CAP; and (iii) a 1.5–3 s
355 TWT thick SF3 unit that contains reflections with variable dips, including prominent swarms
356 of landward-dipping reflections that cross-cut but do not offset other reflections and that
357 typically occur at the oceanward termination of SF1 wedges (Fig. 8). Derivation of interval
358 velocities from seismic reflection stacking velocities suggests rocks comprising SF1 have
359 velocities of ~2.5–5.3 km s⁻¹ (see insets in Fig. 8C) (Goncharov & Nelson 2012). It is
360 difficult to determine whether SF1-SF3 continue across the full extent of the Wallaby Saddle
361 in s310-59 because across its western portion there appears to be a distinct change in
362 reflection configuration (Fig. 8C). In particular, we observe that although there is less
363 reflectivity in this western portion, reflections towards the top of the crust are broadly sub-
364 parallel to the basement reflection and those within the mid- to lower-crustal areas are either
365 gently inclined landwards, or moderately inclined oceanwards (Fig. 8C).

366 Seismic reflection imaging of the Wallaby Plateau reveals the crust is up to ~7 s TWT
367 thick (e.g., at the Sonne Ridge), apparently thicker than that of the Wallaby Saddle (~5–6 s
368 TWT thick) but that there is no apparent significant change in Moho depth between the two
369 crustal domains (Figs 7 and 8); we note these observations are based on time-migrated data
370 and may thus be invalidated if there are differences in velocity structure between the two
371 areas not previously recognised. The crust of the Wallaby Plateau is also thicker than that of
372 the CAP, and its underlying Moho is located at deeper levels (~12 s TWT; Fig. 7). Towards
373 the SW margin of the Wallaby Plateau, a ~40 km wide, apparently NE-trending rift system
374 occurs, comprising normal faults with throws of up to ~1 s TWT that bound and dissect a

375 graben (Figs 8B–D). Reflections within the upper section of the Wallaby Plateau crust are
376 typically moderate-to-high amplitude and form layered packages, which are either
377 conformable to the top basement horizon or that diverge (Fig. 8). The diverging packages of
378 dipping reflections appear similar to SF1 observed in the CAP and Wallaby Saddle (Figs 5
379 and 8). Derivation of interval velocities from seismic reflection stacking velocities suggests
380 rocks comprising these diverging reflector sequences have velocities of $\sim 2.5\text{--}5.3\text{ km s}^{-1}$ (Fig.
381 8C) (Goncharov & Nelson 2012). Due to uncertainties regarding the reliability of seismic
382 processing within the middle and lower crustal sections of the Wallaby Plateau, e.g., where
383 imaging is hindered by seabed multiples, it is difficult to confidently interpret reflections as
384 real geological features and not artefacts. However, we note that in these middle and lower
385 crustal sections, reflections are low-to-moderate amplitude and broadly dip gently in various
386 directions; in places, steeply inclined reflections are observed that appear to cross-cut but not
387 offset gently dipping reflections (Fig. 8). These steeply inclined mid- to lower-crustal
388 reflections typically appear to be located beneath diverging reflection packages, or beyond
389 their down-dip termination (Fig. 8).

390

391 *Comparison of magnetic anomalies to seismic reflection data*

392 EMAG2v2 and ship-track magnetic data reveal that 10 km wide, ≤ 220 km long magnetic
393 stripes cover much of the CAP (Figs 1B, C, 4, and 5). No magnetic stripes can confidently be
394 identified and dated within the Wallaby Plateau and none are observed within the Wallaby
395 Saddle (Figs 1B, C, and 4). Although magnetic anomalies in the EMAG2v3 grid are
396 suppressed relative to EMAG2v2, subtle, linear anomalies can still be distinguished across
397 the CAP and in the Gallah Province (cf. Figs 4A and B). Because we identify no ridge-like
398 feature where Gibbons et al. (2012) inferred an extinct seafloor spreading centre, we discard
399 their assignation of magnetic chron ages and instead compare our seismic reflection data to

400 those of Robb et al. (2005). In particular, proximal to the Australian continent, long-
401 wavelength magnetic anomalies can only be broadly assigned to chron M10N (~135.9–134.2
402 Ma; Figs 1B, 4, and 5) (Robb et al. 2005); across parts of seismic lines EW0113-5, EW0113-
403 6, and repro-n303, chrons M10n–M5r (~135.3–131.4 Ma) are clearly defined and have
404 amplitudes of $\leq \pm 100$ nT (Figs 1B, 4, and 5). There is no apparent correlation between the
405 distribution of seaward-dipping reflector sequences in SF1 or thickness variations in any of
406 the three seismic facies to the location or intensity of the magnetic chrons (Fig. 5). However,
407 we note that on all three seismic lines, chrons M8r–M7n (~133–132 Ma) coincide with a
408 package of seaward-dipping reflectors observed in SF1, which on EW0113-5 is ≤ 3 km thick
409 and ~25 km long (Fig. 5). Furthermore, our comparison also shows that individual seaward-
410 dipping reflector sequences can extend across multiple magnetic chrons (Fig. 5).

411

412 *Geochemistry of basalts dredged from the Sonne Ridge*

413 The only basalt collected from the Sonne Ridge displays a relatively flat Rare Earth Element
414 (REE) pattern and has been previously described as having a slightly enriched MORB-like
415 source (Fig. 9A) (Dadd et al. 2015). By replotting the trace element and radiogenic isotopic
416 compositions of the altered Sonne Ridge sample, we show the sample: (i) displays prominent
417 enrichments in Rb, K, and Pb relative to average enriched MORB (Fig. 9A); (ii) a depletion
418 of Nb relative to average enriched MORB (Fig. 9A); and (iii) an elevated $^{87}\text{Sr}/^{86}\text{Sr}$ and
419 unradiogenic ϵ_{Nd} (Fig. 9B). We also note that the REE pattern defined by the Sonne Ridge
420 basalt appears similar to REE profiles of basalts from the Wallaby Plateau, Globally
421 Subducting Sediment (GLOSS), and average continental crust (Fig. 9A).

422

423 **Interpretation**

424 *Seismic facies*

425 Beneath the sedimentary cover across the CAP, we recognise three distinct layers (SF1–SF3;
426 Figs 5–8). We identify a upper-crustal layer (SF1) in the CAP that comprises well-developed
427 wedges of divergent, seaward-dipping reflectors (SDRs) (Figs 5 and 6). These SDRs are ≤ 4.5
428 km thick, likely have OBS-derived seismic velocities of $\sim 4\text{--}5\text{ km s}^{-1}$ (Tischer 2006), and
429 collectively extend >300 km west of the previously interpreted oceanward limit of the Cuvier
430 Margin COTZ (Figs 1A, 5, and 6). Diverging SDRs are also observed within: (i) the
431 previously defined, 50–70 km wide COTZ along the Cuvier Margin beneath the continental
432 slope, where they are up to ~ 5 km thick (e.g., Fig. 1D) (e.g., Hopper et al. 1992; Symonds et
433 al. 1998); and (ii) across the Wallaby Saddle and Wallaby Plateau, where they are $\sim 5\text{--}10$ km
434 thick and have seismic stacking velocities of $2.5\text{--}5.3\text{ km s}^{-1}$ (Fig. 8) (e.g., Symonds et al.
435 1998; Sayers et al. 2002; Goncharov & Nelson 2012). The lack of boreholes penetrating these
436 SDR sequences offshore NW Australia means we cannot determine their composition or the
437 nature of underlying crust. However, SDR sequences that are geometrically and
438 geophysically similar to those from offshore NW Australia (e.g., SF1) have been recognised
439 along other passive margins, where they are developed on either heavily intruded continental
440 crust or thickened oceanic crust (e.g., Hinz 1981; Larsen & Saunders 1998; Harkin et al.
441 2020). Where these SDRs have been drilled, or are exposed onshore (e.g., Iceland and
442 Greenland), they comprise interbedded basaltic lavas, tuffs, and sedimentary rocks formed
443 during sub-aerial, or perhaps shallow-water, continental breakup and crustal spreading (e.g.,
444 Bodvarsson & Walker 1964; Mutter et al. 1982; Roberts et al. 1984; Eldholm et al. 1987;
445 Larsen et al. 1994a; Geoffroy et al. 2001; Harkin et al. 2020). Based on similarities in
446 structure and seismic velocities to SDRs studied elsewhere, we suggest that SF1 comprises
447 spreading-related volcanic rocks interbedded with sedimentary layers (Figs 1D, 5, 6, and 8)
448 (e.g., Mutter et al. 1982; Hopper et al. 1992; Symonds et al. 1998; Planke et al. 2000;
449 McDermott et al. 2019; Harkin et al. 2020).

450 The observed structure and seismic velocities (6.8–7.2 km s⁻¹) of SF2 and SF3 in the
451 CAP, defined by transparent seismic facies and discordant high-amplitude reflections,
452 respectively (Figs 5–8), are consistent with the typical seismic character of sheeted dykes and
453 lower crustal gabbro intrusions in oceanic crust (e.g., Eittreim et al. 1994; Paton et al. 2017).
454 However, we note that these seismic facies are not uniquely diagnostic of oceanic crust but
455 can also occur in COTZs, where moderate- to high-amplitude reflections may represent
456 igneous intrusions (e.g., dykes and sills), primary layering within gabbros, or texturally
457 distinct lower crustal shear zones within otherwise homogenous crystalline rocks (e.g.,
458 Phipps-Morgan & Chen 1993; Abdelmalak et al. 2015; Paton et al. 2017). For example, the
459 swarm of landward dipping reflections within SF2 and SF3 at the down-dip termination of an
460 SDR sequence may correspond to dykes; i.e. they cross-cut but do not offset background
461 reflections and are thus not faults or shear zones (e.g., Figs 5 and 8) (e.g., Abdelmalak et al.,
462 2015; Phillips et al., 2018).

463

464 *Geochemistry of basalts dredged from the Sonne Ridge*

465 Given the Sonne Ridge basalt displays a relatively flat REE profile (Fig. 9A), Dadd et al.
466 (2015) interpreted it to have a slightly enriched MORB-like source and thus supported the
467 inference that the CAP comprises oceanic crust (e.g., Larson et al. 1979; Hopper et al. 1992;
468 Mihut & Müller 1998). However, borehole data from a COTZ within the South China Sea
469 suggests igneous rocks produced during its formation are MORB-like, implying such a
470 chemical signature is not indicative of oceanic crust (Nirrengarten et al. 2020). Furthermore,
471 although a flat REE pattern can be indicative of a garnet-free melting regime, such as where a
472 majority of melt is generated in a MORB setting, it does not preclude other settings. It should
473 be noted that the Sonne Ridge submarine sample is heavily altered (Dadd et al. 2015), which
474 may explain the observed elemental enrichment in fluid mobile elements such as Pb and Rb,

475 as well as its elevated $^{87}\text{Sr}/^{86}\text{Sr}$. However, the sample also exhibits unradiogenic ϵ_{Nd} outside
476 the isotopic compositions typical of MORB (Fig. 9B), and a negative anomaly in the fluid
477 immobile, high field strength element Nb, which is in part defined by a relative enrichment in
478 the neighbouring element Th. It is plausible that the negative Nb anomaly and unradiogenic
479 ϵ_{Nd} may indicate a chemically evolved, continental or sedimentary contribution to the
480 magmas. Furthermore, the chemical similarity of the Sonne Ridge basalt to two ~124 Ma
481 samples from the Wallaby Plateau (Fig. 9), which is interpreted to comprise intruded
482 continental crust (Daniell et al. 2009; Stilwell et al. 2012; Olierook et al. 2015), could be
483 considered consistent with a continental or sedimentary contribution to the Sonne Ridge
484 magmas. Overall, our reinterpretation of the single available, highly altered basalt from the
485 Sonne Ridge highlights that its chemistry does not provide conclusive evidence for the origin
486 of the CAP (cf. Dadd et al. 2015).

487

488 **Discussion**

489 Since its magnetic stripes were identified, the CAP has been considered to comprise
490 unambiguous oceanic crust that formed at ~136–134 Ma (Valanginian) in response to
491 seafloor spreading at the Sonne Ridge (e.g., Fig. 10A) (e.g., Falvey & Veevers 1974; Larson
492 et al. 1979; Hopper et al. 1992; Robb et al. 2005; Gibbons et al. 2012). An oceanic origin for
493 the CAP has been supported by seismic reflection-based observations that it has a thin crust
494 relative to adjacent continental blocks (e.g., Fig. 1D) (e.g., Hopper et al. 1992), and chemical
495 data, which suggest it has a MORB-like signature (Dadd et al. 2015). The apparent certainty
496 that the CAP is oceanic means it has been unquestionably treated as such in all geological
497 models of the evolution of NW Australia, including regional and global plate kinematic
498 reconstructions (e.g., Heine & Müller 2005; Gibbons et al. 2012). However, the identification
499 of linear magnetic anomalies within non-oceanic crust, in areas such as Ethiopia and the

500 Atlantic margins (e.g., Bronner et al. 2011; Bridges et al. 2012; Collier et al. 2017;
501 McDermott et al. 2018), prompts a reassessment of the nature of the crust defining the CAP.

502

503 *Implications of SDR recognition for the CAP*

504 *Origin of SDR lavas*

505 Lavas within SDR wedges are inferred to emanate from and be thickest at axial magmatic
506 segments, where they are likely fed by sub-vertical dykes (e.g., Abdelmalak et al. 2015;
507 Norcliffe et al. 2018). With continued plate divergence, these lavas subside and rotate to dip
508 inwards towards their eruption site (e.g., Planke & Eldholm 1994; Paton et al. 2017; Norcliffe
509 et al. 2018; Tian & Buck 2019); this subsidence also rotates underlying feeder dykes, which
510 will thus dip away from the magmatic segment (e.g., Lenoir et al. 2003; Abdelmalak et al.
511 2015). SDRs across the CAP appear to dip and diverge north-westwards, except one SDR-
512 like package of concave-upwards reflections that borders and diverges south-eastwards
513 towards the Sonne Ridge; i.e. we define a conjugate set of SDRs that occur either side of and
514 dip towards the Sonne Ridge (Fig. 5). Although only one SDR package to the NW of the
515 Sonne Ridge dips south-eastwards towards the ridge, we suggest that the other SDR
516 packages, which dip north-westwards, relate to and were formed at the Sonja Ridge (Fig. 5).
517 We also note that along EW0113-5 and EW0113-6 there are no changes in SDR divergence
518 direction, as well as no localised increase in crustal thickness or elevated basement, where
519 Gibbons et al. (2012) proposed the CAP spreading ridge was located (Figs 1C, 5A, and B).
520 Given this lack of evidence for a spreading ridge ~100 km SE of the Sonne Ridge, we
521 discount the crustal and magnetic chron configuration of Gibbons et al. (2012), and instead
522 follow that presented by Robb et al. (2005) (cf. Figs 1B, C, and 10A).

523 Overall, from the SDR geometries and distribution we describe, coupled with the
524 previously inferred conjugate sets of magnetic chrons (Fig. 1B), our results are consistent

525 with suggestions that: (i) extension within the CAP was predominantly centred on the Sonne
526 Ridge during chrons M10N–M5r (~136–131 Ma); before (ii) briefly jumping to the Sonja
527 Ridge at ~131 Ma (chron M5n), which interrupted subsidence and rotation of the SDR wedge
528 immediately to the NW of the Sonne Ridge and instead produced north-westwards diverging
529 SDRs (Falvey & Veevers 1974; Larson et al. 1979; Robb et al. 2005; MacLeod et al. 2017).
530 Our reinterpretation of the Sonne Ridge basalt indicates its chemical signature cannot be used
531 to conclusively define whether the Sonne Ridge represents an oceanic or intra-COTZ
532 spreading centre (Dadd et al. 2015).

533

534 *Environment of SF1 lava emplacement*

535 Borehole and field data reveal SDR lavas typically erupt sub-aerially, but can develop sub-
536 aqueously (e.g., Bodvarsson & Walker 1964; Mutter et al. 1982; Roberts et al. 1984; Eldholm
537 et al. 1987; Larsen et al. 1994b; Symonds et al. 1998; Planke et al. 2000; Geoffroy et al.
538 2001; Harkin et al. 2020). Determining the environment and age of SDR formation can help
539 establish whether they likely formed via: (i) seafloor spreading at a mid-ocean ridge,
540 consistent with previous interpretations that the CAP comprises unambiguous oceanic crust
541 (e.g., Falvey & Veevers 1974; Larson et al. 1979; Hopper et al. 1992; Robb et al. 2005); or
542 (ii) magmatic addition along a sub-aerial or shallow-water axis during the transition from
543 continental rifting to full plate separation (e.g., McDermott et al. 2018), implying the CAP
544 does not comprise oceanic crust. However, from their seismic character alone it can be
545 difficult to determine whether SDRs formed in sub-aerial, shallow-water, or deep-marine
546 environments (e.g., compare inner and outer SDR character and inferred emplacement
547 conditions; Symonds et al. 1998; Planke et al. 2000).

548 Observations from the DSDP Site 263 borehole, which terminates ~100–200 m above
549 the CAP crystalline crust, indicate the sedimentary cover deposited above the SDRs: (i)

550 comprises poorly sorted silty claystones that include angular quartz grains and abundant
551 kaolinite, consistent with a neritic (i.e. <200 m water depth) depositional environment (Fig.
552 3B) (e.g., Robinson et al. 1974; Veevers & Johnstone 1974; Compton et al. 1992; Holbourn
553 & Kaminski 1995; Oosting et al. 2006); (ii) contain coarsely agglutinated foraminifera
554 species and taxa such as *Hyperamina* spp. within the lowermost intersected strata, which are
555 typical of shallow-marine conditions (Holbourn & Kaminski 1995); and (iii) based on
556 biostratigraphic data were deposited at least in the middle Barremian (e.g., ~127 Ma), but are
557 perhaps as old as Hauterivian (~132.6–129.4 Ma) (Oosting et al. 2006). As DSDP Site 263
558 occurs above crust recording chron M10N (135.9–134.2 Ma), these age constraints suggest
559 local deposition of the lowermost sedimentary cover occurred up to ~9 Myr (i.e. ~135.9–127
560 Ma) later than the underlying basement, concurrent with development of crust hosting chrons
561 M7–M1n (132.5–126.3 Ma). Crust hosting chrons M7–M1n is located >100 km to the NW of
562 chron M10N (Fig. 1B). Critically, SDR-bearing crust cools and subsides as it is transported
563 away from its emplacement site, leading to rotation of the SDR sequence (e.g., Planke &
564 Eldholm 1994; Paton et al. 2017; Norcliffe et al. 2018; Tian & Buck 2019). The presence of
565 strata deposited in the neritic zone above SF1 in DSDP 263, after ~9 Myr of crustal cooling
566 and subsidence, thus implies lava eruption during the early stages of CAP formation
567 occurred: (i) in a sub-aerial or shallow-water environment (i.e. comparable to the inner SDRs
568 of Symonds et al. 1998; Planke et al. 2000), if we assume the underlying crust only subsided
569 in the ~9 Myr between SDR emplacement and sediment deposition; or (ii) at a moderately
570 deep-marine spreading centre (i.e. comparable to the outer SDRs of Symonds et al. 1998;
571 Planke et al. 2000), but localised uplift elevated the DSDP 263 area to bathymetric depths
572 equivalent to the neritic zone prior to deposition of overlying strata. We lack the data from
573 strata directly overlying or interbedded with the SDRs to test these two interpretations
574 regarding lava emplacement depth, but note that the relatively flat-lying crystalline crust

575 across the interpreted CAP seismic lines (except for the Sonne Ridge) provides no evidence
576 of post-spreading uplift, perhaps suggesting a sub-aerial or shallow-water environment of
577 emplacement is most plausible (Fig. 5).

578

579 *Nature of CAP crust*

580 Seismic and magnetic data alone are insufficient to determine the origin of the CAP crust
581 because the SDRs, seismic facies (SF1–SF3), and magnetic stripes these data illuminate can
582 manifest in both oceanic crust and COTZs (e.g., Larsen & Saunders 1998; Symonds et al.
583 1998; Planke et al. 2000; Bridges et al. 2012; Collier et al. 2017; McDermott et al. 2018). We
584 also show that the chemical data available for a basalt from the Sonne Ridge may possess a
585 continental signature, and is thus inconclusive regarding whether or not the crust is oceanic
586 (Fig. 9) (cf. Dadd et al. 2015). Instead, based on lithological and biostratigraphic data from
587 the sedimentary cover intersected by DSDP Site 263, we suggest it may be possible that: (i)
588 the inferred lavas within SF1, at least during the early stages of CAP formation (i.e. chron
589 M10N), erupted in a sub-aerial, or perhaps shallow-water (<200 m water depth),
590 environment; and (ii), assuming the underlying crystalline crust had since subsided relative to
591 its formation position, that during deposition of sedimentary cover on crust recording chron
592 M10N, the contemporaneous, ~9 Myr old Sonne Ridge was elevated above at least the base
593 of the neritic zone. These potential constraints on SDR emplacement depth are inconsistent
594 with the CAP being oceanic crust since mid-ocean ridges in such a setting are expected to
595 occur at water depths of ~3 km after 5–10 Myr of spreading (e.g., Menard 1969; Parsons &
596 Sclater 1977; Stein & Stein 1992).

597 From the distribution of the magnetic chrons (Fig. 1B) and the probable sub-aerial or
598 shallow-water elevation of the ridge during extension, we propose currently available
599 information is consistent with the CAP comprising a COTZ (Fig. 10B). In particular, we

600 suggest the CAP could record a gradual north-westwards change from the continental crust of
601 the Cuvier Margin into heavily intruded continental crust, and progressively becomes
602 increasingly magma-dominated towards the Sonne Ridge (Figs 2, 10B, and C). Our data are
603 insufficient to determine where, or if, there is a transition from heavily intruded continental
604 crust to magmatic crust, which would mark break-up of the continental crust within the CAP.
605 Our proposed alternative model implies that full continental lithospheric rupture may not
606 have occurred in the CAP; we currently lack data constraining the nature of the CAP crust
607 bearing chron M5n adjacent to the Sonja Ridge or detailed enough to model residual
608 bathymetric anomalies to fully test this hypothesis (Figs 10B and C).

609 Repetition of the M10N-M6 chrons centred on the Sonne Ridge suggests the possible
610 COTZ of the CAP may extend at least out to chron M3n, which is recorded by inferred
611 unambiguous oceanic crust situated: (i) >500 km oceanwards of the outer- limit of the
612 previously defined Cuvier COTZ (e.g., Hopper et al. 1992; Symonds et al. 1998); and (ii)
613 broadly coincident with the north-western limit of the Gallah Province on the Gascoyne
614 margin (Direen et al. 2008) (Figs 1B and 10B). We suggest rupture of the continental
615 lithosphere and onset of seafloor spreading could have occurred simultaneously offshore the
616 Cuvier and Gascoyne margins at ~131 Ma (Hauterivian), following an oceanwards ridge
617 jump from the Sonja Ridge, producing unambiguous oceanic crust recording chron M3n
618 (Figs 10B and C) (e.g., Robb et al. 2005; Direen et al. 2008). Continuation of the COTZ
619 across the CAP has implications for the timing and kinematics of plate reconstructions of the
620 NW Australian margin, with the onset of deep-marine seafloor spreading potentially ~3 Myr
621 later than suggested by previous studies (e.g., Robb et al. 2005).

622 Interpreting the CAP as a COTZ developed through sub-aerial, or at least shallow-
623 water, extension implies its crust was: (i) thicker during SDR emplacement, but concurrently
624 and/or subsequently thinned during continued magmatic extension and late-stage stretching

625 (e.g., Bastow & Keir 2011; Bastow et al. 2018); (ii) less dense and thus more buoyant than
626 unambiguous oceanic crust, because it likely retained a significant proportion of continental
627 material; and (iii) thermally buoyant due to the presence of abundant hot intrusions and
628 underlying, decompressing mantle. That these processes can maintain rift axes at above or
629 near sea-level elevations is demonstrated by the onshore occurrence of active rift zones,
630 characterised by heavily-intruded continental crust, in the Main Ethiopia Rift and Afar (e.g.,
631 Hayward & Ebinger 1996; Ebinger & Casey 2001; Mackenzie et al. 2005; Bridges et al.
632 2012).

633 Because the degree of thermal subsidence is at least partly controlled by crustal
634 density, we would expect oceanic crust to thermally subside more than less dense, heavily-
635 intruded continental crust. Given the Hauterivian-to-Middle Barremian sedimentary strata
636 overlying the SDRs were deposited in neritic conditions (Veevers & Johnstone 1974;
637 Holbourn & Kaminski 1995; Oosting et al. 2006), it is apparent the CAP subsided from near
638 sea-level to a current, unloaded basement depth of ~6.5 km; this total subsidence is greater
639 than predicted for dense, thermally subsiding oceanic crust (Stein & Stein 1992). To interpret
640 the CAP as COTZ crust, our results would require other mechanisms, in addition to thermal
641 subsidence, to influence its subsidence history. For example, post-breakup decay of
642 asthenospheric thermal anomalies may account for some elevation discrepancies via removal
643 of dynamic support of the margin (e.g., Czarnota et al. 2013). Finally, the CAP COTZ may
644 have involved some late-stage stretching prior to terminal breakup and the onset of seafloor
645 spreading, akin to processes observed today in the sub-aerial Red Sea rift in Ethiopia (e.g.,
646 Bastow & Keir 2011; Daniels et al. 2014).

647

648 *Development of magnetic stripes during break-up*

649 Recent forward modelling of conjugate, ship-track magnetic profiles by Collier et al. (2017)
650 suggest magnetic signals over SDRs arise from a combination of stacked and rotated lavas,
651 producing a long-wavelength positive anomaly that can sometimes mask reversals, and linear
652 magnetic anomalies caused by dyke intrusion in the underlying crust. Stacked SDR wedges
653 on the CAP are part of a possible COTZ and span several chrons (e.g. M8n-M7r), but are
654 ≤ 4.5 km thick (Figs 5 and 6). These observations indicate the CAP magnetic stripes likely
655 record magnetic reversal signatures originating from sub-SDR rocks; i.e. the SDRs and flat-
656 lying lavas are too thin to dominate the magnetic signature (cf. Collier et al. 2017). In
657 contrast, the less-clearly developed yet higher amplitude magnetic reversals in the Gallah
658 Province COTZ may relate to interference from the greater SDR thicknesses (≤ 5.5 km)
659 relative to the CAP (Direen et al. 2008). Our inference that the magnetic signature is derived
660 from sub-SDR rocks is also consistent with studies of onshore incipient spreading centres
661 (e.g. Ethiopia), where magnetic stripes likely originate from axial intrusion by dykes in
662 heavily intruded, upper continental crust, rather than overlying lavas (Bridges et al. 2012).

663 We suggest that SDR thickness and, thereby, preservation of magnetic anomalies
664 within a COTZ can partly be attributed to extension rate. For example, the extension rate
665 during SDR eruption offshore NW Australia (~ 4.5 cm/yr half rate; Robb et al. 2005) is
666 substantially faster than the inferred extension rates for the South Atlantic during magmatic
667 crust formation (~ 1.1 cm/yr half-rate; Paton et al. 2017). Slower extension rates (e.g. South
668 Atlantic) likely promote stacking of lava flows to produce thicker SDRs (Eagles et al. 2015),
669 leading to interference between the magnetic signal of the SDRs and sub-SDR crust and thus
670 the development of the long-wavelength positive magnetic anomalies (e.g., Moulin et al.
671 2010). Extension rate may also influence magnetic anomaly development by affecting the
672 width of magnetic stripes; reversal anomalies will be narrowest at slow spreading ridges

673 (Vine 1966). The narrower anomalies, combined with the greater potential for vertical
674 stacking of lavas, will tend to hinder the interpretation of magnetic anomalies.

675

676 **Conclusions**

677 The recognition of magnetic stripes within the Cuvier Abyssal Plain (CAP), offshore NW
678 Australia, has led to the assumption that it comprises oceanic crust generated by conventional
679 seafloor spreading at the Sonne Ridge, probably at water depths of ≥ 2 km. We challenge this
680 assumption, in line with the growing consensus that magnetic stripes are not necessarily
681 diagnostic of oceanic crust and can also form in continent-ocean transition zones (COTZs).
682 Using regional 2D seismic reflection lines we demonstrate that the uppermost layer in the
683 CAP crystalline crust contains seaward-dipping reflector (SDR) sequences, akin to those
684 observed in the previously defined COTZ of the Cuvier Margin and Wallaby Saddle, as well
685 as on the heavily intruded continental crust of the Wallaby Plateau. Through comparison to
686 SDRs recognised elsewhere, we suggest those observed across the CAP comprise lavas,
687 interbedded with sedimentary strata, erupted from an axial magmatic segment. Lithological
688 and biostratigraphic data from a borehole penetrating the CAP sedimentary cover, which
689 were deposited in neritic (<200 m water depth) conditions, require the underlying crystalline
690 crust to have been at shallow-water depths ~ 9 Myr after its formation and thus imply SDR
691 emplacement occurred in a shallow water or sub-aerial environment. We also reinterpret
692 chemical data from a basalt dredged along the Sonne Ridge, showing it cannot be
693 conclusively attributed to a MORB setting as previously interpreted. Overall, these data and
694 interpretations suggest the CAP may not comprise unambiguous oceanic crust, but could
695 instead represent a >500 km wide COTZ where extension likely became more magma-
696 dominated, producing heavily-intruded continental crust (akin to present-day Ethiopia) at its
697 landward edge through to magmatic crust formed by sub-aerial or shallow-marine spreading

698 at the Sonne and Sonja ridges. In our conceptual model, break-up of the continental crust
699 could have occurred during the formation of the CAP, but full continental lithospheric
700 rupture occurred outboard of the COTZ following a ridge jump at ~130 Ma. Our re-
701 evaluation of the CAP crustal type supports suggestions that COTZs along volcanic passive
702 margins may record the development of magnetic stripes, which thus should not be used
703 alone as a reliable proxy for the onset of seafloor spreading and the extent of oceanic crust.

704

705 **Acknowledgements**

706 Schlumberger are thanked for provision of Petrel software licenses. M.T.R. was supported by
707 NERC grant NE/L501621/L. The EW0113 seismic survey (DOI: 10.1594/IEDA/500095) and
708 EMAG2 magnetic anomaly grids were, and can be downloaded from, the Marine Geoscience
709 Data System and the NOAA National Geophysical Data Centre, respectively. Gwenn Peron-
710 Pinvidic, Gareth Roberts, and Saskia Goes are thanked for helpful discussions during the
711 preparation of this manuscript. We thank five reviewers, including Jon Bull, for their
712 constructive comments on previous versions of this manuscript. Finally we are grateful to
713 Amy Gilligan for the editorial handling of this manuscript, and to Lucía Pérez-Díaz and an
714 anonymous reviewer for their constructive comments.

715

716 **Figure captions**

717 Figure 1: (A) Location map of the study area highlighting the seismic lines used in this study
718 and key tectonic elements, including areas of recognised seaward-dipping reflectors (SDRs)
719 (Symonds et al. 1998; Holford et al. 2013) and continent-ocean transition zones (COTZs;
720 Symonds et al. 1998; Direen et al. 2008). Inset: study area location offshore NW Australia.
721 AAP – Argo Abyssal Plain, CAP – Cuvier Abyssal Plain, CRFZ – Cape Range Fracture
722 Zone, GAP – Gascoyne Abyssal Plain, GP – Gallah Province, NCB – North Carnarvon

723 Basin, EP – Exmouth Plateau, PB – Perth Basin, SCB – South Carnarvon Basin, Cu – Cuvier
724 margin COTZ, SR – Sonne Ridge, SjR – Sonja Ridge, WP – Wallaby Plateau, WS – Wallaby
725 Saddle, WZFZ – Wallaby-Zenith Fracture Zone. Dredge sites 52, 55 (samples 055BS004A
726 and 055BS004B), and 57 (sample 057DR051A) are also shown (Dadd et al. 2015). See
727 Supplementary Figure S1 for an uninterpreted version. (B) Total magnetic intensity grid
728 (EMAG2v2), interpreted magnetic chrons based on Robb et al. (2005). See Supplementary
729 Figure S1 for an uninterpreted version. (C) Total magnetic intensity grid (EMAG2v2),
730 interpreted magnetic chrons based on Gibbons et al. (2012). See Supplementary Figure S1 for
731 an uninterpreted version. (C) Uninterpreted and interpreted seismic line (i.e. seismic profile
732 670) across the Cuvier Margin, imaging the crustal structure beneath the continental shelf and
733 the deep abyssal plain (modified from Hopper et al., 1992). Velocity profiles from refraction
734 experiments shown; see Hopper et al., (1992) for details. See Figure 1A for approximate line
735 location and Supplementary Figure S2 for an enlarged version of the uninterpreted seismic
736 line.

737

738 Figure 2: Schematic model (not to scale) of a continent-ocean transition zone along a magma-
739 rich passive margin, which depicts the evolution from unambiguous continental crust to
740 unambiguous oceanic crust. As magma intrudes continental crust, likely as dykes at mid- to
741 upper-crustal levels and larger gabbroic bodies in the lower crust, it becomes ‘heavily
742 intruded continental crust’ (e.g., Eldholm et al. 1989). Continued intrusion and dyking leads
743 to localisation of magmatism within narrow zones where there is little, if any, continental
744 crust remaining (i.e. ‘magmatic crust’; e.g., Collier et al. 2017; Paton et al. 2017). We
745 categorize heavily intruded continental crust and magmatic crust as ‘COTZ crust’. Sub-aerial,
746 magma-assisted rifting may feed extensive lava flows that later, through subsidence, become
747 seaward-dipping reflectors (SDRs). SDR subsidence leads to rotation of underlying dykes

748 (Abdelmalak et al. 2015); a similar rotation of lavas and dykes is observed in oceanic crust
749 (Karson 2019).

750

751 Figure 3: Tectono-stratigraphic chart for the Exmouth Plateau and Cuvier Margin
752 (information from Hocking et al. 1987; Arditto 1993; Partington et al. 2003; Reeve et al.
753 2016). (B) Comparison between stratigraphic data from DSDP 263 and Pendock-1 boreholes
754 (modified from Veevers & Johnstone 1974; Holbourn & Kaminski 1995). See Figure 1A for
755 borehole locations.

756

757 Figure 4: Total magnetic intensity grids EMAG2v2 and EMAG2v3 (Maus et al. 2009; Meyer
758 et al. 2017). The limits of unambiguous continental crust, locations of previously defined
759 COTZs, possible spreading ridges, and seismic lines also shown (see Fig. 1 for legend).

760

761 Figure 5: Interpreted and uninterpreted, depth-converted seismic lines (A) EW0113-5 and (B)
762 EW0113-6, and the time-migrated line (D) repro n303 showing crustal structure of the Cuvier
763 Margin; see Figures 1A and 5C for line locations. The tie-co-located magnetic anomaly
764 profile showing interpreted magnetic chrons is presented for (A–D) (after Robb et al. 2005).
765 See Supplementary Figure S2 for an enlarged version of the uninterpreted seismic lines.

766

767 Figure 6: Zoomed in view of EW0113-5 highlighting the seismic character of interpreted
768 SDR packages (see Fig. 5A for location).

769

770 Figure 7: Interpreted and uninterpreted, time-migrated seismic line s135-11; see Figure 1A
771 for location. See Supplementary Figure S2 for an enlarged version of the uninterpreted
772 seismic line.

773

774 Figure 8: Interpreted and uninterpreted, time-migrated seismic lines (A) s135-s135_05, (B)
775 s135-08, and (D) s310-59 showing crustal structure of the Wallaby Plateau and Wallaby
776 Saddle; see Figures 1A and 8D for line locations. See Supplementary Figure S2 for an
777 enlarged version of the uninterpreted seismic lines.

778

779 Figure 9: (A) Primitive mantle normalized incompatible element diagram comparing the
780 dredged Sonne Ridge and Wallaby Plateau basalt lava samples with average (ave.)
781 compositions of MORB variants (Hofmann 2014), Globally Subducting Sediment (GLOSS)
782 (Plank & Langmuir 1998), and continental crust (Rudnick & Fountain 1995). Primitive
783 mantle normalisation factors from (Sun & McDonough 1989). (B) Plot of $\epsilon(\text{Nd})$ versus
784 $^{87}\text{Sr}/^{86}\text{Sr}$, illustrating that the Sonne Ridge and Wallaby Plateau samples are distinct from
785 MORB (based on data collated in Hofmann 2014). Both measured and initial $^{87}\text{Sr}/^{86}\text{Sr}$ ratios
786 are given in Dadd et al. (2015). It is unclear if the reported $^{143}\text{Nd}/^{144}\text{Nd}$ in Dadd et al. (2015)
787 is age corrected or not. We assume that they are not, and plot both age corrected and
788 measured Sr-Nd isotopic compositions.

789

790 Figure 10: (A) Map showing the potential limits of the COTZ based on interpreting the CAP
791 and Gallah Province as transitional and/or magmatic crust. (B-D) Schematic maps showing
792 the development of COTZ crust and the onset of oceanic crust accretion adjacent to the
793 Gascoyne and Cuvier margins, during formation of chrons (B) M10, (C) M6 and (D) M3r.
794 See Figure 1 for chron ages. Location of present day coastline shown for reference.

795

796 **References**

797 Abdelmalak, M.M., Andersen, T.B., Planke, S., Faleide, J.I., Corfu, F., Tegner, C., Shephard, G.E.,
798 Zastrozhnov, D., *et al.* 2015. The ocean-continent transition in the mid-Norwegian margin: Insight
799 from seismic data and an onshore Caledonian field analogue. *Geology*, **43**, 1011-1014.

800
801 Arditto, P.A. 1993. Depositional sequence model for the post-Barrow Group Neocomian succession,
802 Barrow and Exmouth sub-basins, Western Australia. *The APPEA Journal*, **33**, 151-160.

803
804 Bastow, I.D. & Keir, D. 2011. The protracted development of the continent-ocean transition in Afar.
805 *Nature Geoscience*, **4**, 248-250.

806
807 Bastow, I.D., Booth, A.D., Corti, G., Keir, D., Magee, C., Jackson, C.A.L., Warren, J., Wilkinson, J.,
808 *et al.* 2018. The Development of Late-Stage Continental Breakup: Seismic Reflection and Borehole
809 Evidence from the Danakil Depression, Ethiopia. *Tectonics*, **37**, 2848-2862.

810
811 Bécél, A., Davis, J.K., Shuck, B.D., Van Avendonk, H.J. & Gibson, J.C. 2020. Evidence for a
812 prolonged continental breakup resulting from slow extension rates at the Eastern North American
813 Volcanic Rifted Margin. *Journal of Geophysical Research: Solid Earth*, **125**, e2020JB020093.

814
815 Bodvarsson, G. & Walker, G. 1964. Crustal drift in Iceland. *Geophysical Journal International*, **8**,
816 285-300.

817
818 Bolli, H.M. 1974. *Jurassic and Cretaceous Calcisphaerulidae from DSDP Leg 27, eastern Indian*
819 *Ocean*.

820
821 Bridges, D.L., Mickus, K., Gao, S.S., Abdelsalam, M.G. & Alemu, A. 2012. Magnetic stripes of a
822 transitional continental rift in Afar. *Geology*, **40**, 203-206.

823
824 Bronner, A., Sauter, D., Manatschal, G., Péron-Pinvidic, G. & Munsch, M. 2011. Magmatic breakup
825 as an explanation for magnetic anomalies at magma-poor rifted margins. *Nature Geoscience*, **4**, 549.

826
827 Cannat, M., Sauter, D., Lavier, L., Bickert, M., Momoh, E. & Leroy, S. 2019. On spreading modes
828 and magma supply at slow and ultraslow mid-ocean ridges. *Earth and Planetary Science Letters*, **519**,
829 223-233.

830
831 Causer, A., Pérez-Díaz, L., Adam, J. & Eagles, G. 2020. Uncertainties in break-up markers along the
832 Iberia–Newfoundland margins illustrated by new seismic data. *Solid Earth*, **11**, 397-417.

833
834 Collier, J.S., McDermott, C., Warner, G., Gyori, N., Schnabel, M., McDermott, K. & Horn, B.W.
835 2017. New constraints on the age and style of continental breakup in the South Atlantic from
836 magnetic anomaly data. *Earth and Planetary Science Letters*, **477**, 27-40.

837
838 Colwell, J., Symonds, P. & Crawford, A. 1994. The nature of the Wallaby (Cuvier) Plateau and other
839 igneous provinces of the west Australian margin. *Journal of Australian Geology and Geophysics*, **15**,
840 137-156.

841

- 842 Compton, J., Mallinson, D., Netranatawong, T. & Locker, D. 1992. *Regional correlation of*
843 *mineralogy and diagenesis of sediment from the Exmouth Plateau and Argo Basin, Northwestern*
844 *Australian Continental Margin.*
- 845
846 Corti, G., Agostini, A., Keir, D., Van Wijk, J., Bastow, I.D. & Ranalli, G. 2015. Magma-induced axial
847 subsidence during final-stage rifting: Implications for the development of seaward-dipping reflectors.
848 *Geosphere*, **11**, 563-571.
- 849
850 Czarnota, K., Hoggard, M., White, N. & Winterbourne, J. 2013. Spatial and temporal patterns of
851 Cenozoic dynamic topography around Australia. *Geochemistry, Geophysics, Geosystems*, **14**, 634-
852 658.
- 853
854 Dadd, K.A., Kellerson, L., Borissova, I. & Nelson, G. 2015. Multiple sources for volcanic rocks
855 dredged from the Western Australian rifted margin. *Marine Geology*, **368**, 42-57.
- 856
857 Daniell, J., Jorgensen, D., Anderson, T., Borissova, I., Burq, S., Heap, A., Hughes, D., Mantle, D., *et*
858 *al.* 2009. Frontier basins of the West Australian continental margin. *Geoscience Australia Record*, **38**,
859 243.
- 860
861 Daniels, K.A., Bastow, I.D., Keir, D., Sparks, R.S.J. & Menand, T. 2014. Thermal models of dyke
862 intrusion during development of continent–ocean transition. *Earth and Planetary Science Letters*,
863 **385**, 145-153.
- 864
865 Direen, N.G., Stagg, H.M.J., Symonds, P.A. & Colwell, J.B. 2008. Architecture of volcanic rifted
866 margins: new insights from the Exmouth – Gascoyne margin, Western Australia. *Australian Journal*
867 *of Earth Sciences*, **55**, 341-363.
- 868
869 Direen, N.G., Borissova, I., Stagg, H., Colwell, J.B. & Symonds, P.A. 2007. Nature of the continent–
870 ocean transition zone along the southern Australian continental margin: a comparison of the
871 Naturaliste Plateau, SW Australia, and the central Great Australian Bight sectors. *In*: Karner, G.D.,
872 Manatschal, G. & Pinheiro, L. (eds) *Imaging, Mapping and Modelling Continental Lithosphere*
873 *Extension and Breakup*. Geological Society, London, Special Publications, **282**, 239-263.
- 874
875 Eagles, G., Pérez-Díaz, L. & Scarselli, N. 2015. Getting over continent ocean boundaries. *Earth-*
876 *Science Reviews*, **151**, 244-265.
- 877
878 Ebinger, C.J. & Casey, M. 2001. Continental breakup in magmatic provinces: An Ethiopian example.
879 *Geology*, **29**, 527-530.
- 880
881 Eittreim, S.L., Gribidenko, H., Helsley, C.E., Sliter, R., Mann, D. & Ragozin, N. 1994. Oceanic
882 crustal thickness and seismic character along a central Pacific transect. *Journal of Geophysical*
883 *Research: Solid Earth*, **99**, 3139-3145.
- 884
885 Eldholm, O., Thiede, J. & Taylor, E. 1989. The Norwegian continental margin: tectonic, volcanic, and
886 paleoenvironmental framework. *Proceedings of the ocean drilling program, Scientific results*.
887 Citeseer, 5-26.
- 888

- 889 Eldholm, O., Thiede, J., Taylor, E. & Party, S.S. 1987. Summary and preliminary conclusions, ODP
890 Leg 104. *Proceedings of the Ocean Drilling Program, Scientific Results*. Ocean Drilling Program
891 College Station, Texas, 751-771.
- 892
- 893 Falvey, D. & Veevers, J. 1974. Physiography of the Exmouth and Scott plateaus, western Australia,
894 and adjacent northeast Wharton Basin. *Marine Geology*, **17**, 21-59.
- 895
- 896 Geoffroy, L., Callot, J.P., Scaillet, S., Skuce, A., Gélard, J., Ravilly, M., Angelier, J., Bonin, B., *et al.*
897 2001. Southeast Baffin volcanic margin and the North American-Greenland plate separation.
898 *Tectonics*, **20**, 566-584.
- 899
- 900 Gibbons, A.D., Barckhausen, U., den Bogaard, P., Hoernle, K., Werner, R., Whittaker, J.M. & Müller,
901 R.D. 2012. Constraining the Jurassic extent of Greater India: Tectonic evolution of the West
902 Australian margin. *Geochemistry, Geophysics, Geosystems*, **13**, Q05W13.
- 903
- 904 Goncharov, A. & Nelson, G. 2012. From two way time to depth and pressure for interpretation of
905 seismic velocities offshore: Methodology and examples from the Wallaby Plateau on the West
906 Australian margin. *Tectonophysics*, **572**, 26-37.
- 907
- 908 Gradstein, F. & Ogg, J. 2012. The chronostratigraphic scale *The geologic time scale*. Elsevier, 31-42.
- 909
- 910 Harkin, C., Kuszniir, N., Roberts, A., Manatschal, G. & Horn, B. 2020. Origin, composition and
911 relative timing of seaward dipping reflectors on the Pelotas rifted margin. *Marine and petroleum*
912 *geology*, **114**, 104235.
- 913
- 914 Hayward, N. & Ebinger, C. 1996. Variations in the along-axis segmentation of the Afar Rift system.
915 *Tectonics*, **15**, 244-257.
- 916
- 917 Heine, C. & Müller, R. 2005. Late Jurassic rifting along the Australian North West Shelf: margin
918 geometry and spreading ridge configuration. *Australian Journal of Earth Sciences*, **52**, 27-39.
- 919
- 920 Hey, R. 1977. A new class of “pseudofaults” and their bearing on plate tectonics: A propagating rift
921 model. *Earth and Planetary Science Letters*, **37**, 321-325.
- 922
- 923 Hinz, K. 1981. A hypothesis on terrestrial catastrophies Wedges of very thick oceanward dipping
924 layers beneath passive continental margins. Their origin and paleoenvironmental significance.
925 *Geologisches Jahrbuch. Reihe E, Geophysik*, 3-28.
- 926
- 927 Hocking, R.M., Moors, H.T. & Van de Graaff, W.E. 1987. *Geology of the carnarvon basin, Western*
928 *Australia*. State Print. Division.
- 929
- 930 Hofmann, A. 2014. Sampling mantle heterogeneity through oceanic basalts: Isotopes and trace
931 elements. In: RW, C. (ed) *The Mantle and Core, Treatise on Geochemistry*. Elsevier-Pergamon,
932 Oxford, 67-101.
- 933

- 934 Holbourn, A.E. & Kaminski, M.A. 1995. Lower Cretaceous benthic foraminifera from DSDP Site
935 263: micropalaeontological constraints for the early evolution of the Indian Ocean. *Marine*
936 *Micropaleontology*, **26**, 425-460.
- 937
- 938 Holford, S.P., Schofield, N., Jackson, C.A.L., Magee, C., Green, P.F. & Duddy, I.R. 2013. Impacts of
939 igneous intrusions on source and reservoir potential in prospective sedimentary basins along the
940 western Australian continental margin. In: Keep, M. & Moss, S.J. (eds) *The Sedimentary Basins of*
941 *Western Australia IV*. Proceedings of the Petroleum Exploration Society of Australia Symposium,
942 Perth, WA.
- 943
- 944 Hopper, J.R., Mutter, J.C., Larson, R.L. & Mutter, C.Z. 1992. Magmatism and rift margin evolution:
945 Evidence from northwest Australia. *Geology*, **20**, 853-857.
- 946
- 947 Karson, J.A. 2019. From Ophiolites to Oceanic Crust: Sheeted Dike Complexes and Seafloor
948 Spreading. In: Srivastava, R., Ernst, R. & Peng, P. (eds) *Dyke Swarms of the World: A Modern*
949 *Perspective*. Springer, 459-492.
- 950
- 951 Keranen, K., Klemperer, S., Gloaguen, R. & Group, E.W. 2004. Three-dimensional seismic imaging
952 of a protoridge axis in the Main Ethiopian rift. *Geology*, **32**, 949-952.
- 953
- 954 Larsen, H. & Saunders, A. 1998. 41. Tectonism and volcanism at the Southeast Greenland rifted
955 margin: a record of plume impact and later continental rupture. *Proceedings of the Ocean Drilling*
956 *Program, Scientific Results*, 503-533.
- 957
- 958 Larsen, H., Saunders, A. & Clift, P. 1994a. Proceedings of the Ocean Drilling Program, Initial
959 Reports. *Ocean Drilling Program*, College Station, Texas, 1-152.
- 960
- 961 Larsen, H., Saunders, A., Larsen, L. & Lykke-Andersen, H. 1994b. ODP activities on the South-East
962 Greenland margin: Leg 152 drilling and continued site surveying. *Rapport Grønlands Geologiske*
963 *Undersøgelse*, **160**, 75-81.
- 964
- 965 Larson, R.L., Mutter, J.C., Diebold, J.B., Carpenter, G.B. & Symonds, P. 1979. Cuvier Basin: a
966 product of ocean crust formation by Early Cretaceous rifting off Western Australia. *Earth and*
967 *Planetary Science Letters*, **45**, 105-114.
- 968
- 969 Lenoir, X., Féraud, G. & Geoffroy, L. 2003. High-rate flexure of the East Greenland volcanic margin:
970 constraints from ⁴⁰Ar/³⁹Ar dating of basaltic dykes. *Earth and Planetary Science Letters*, **214**, 515-
971 528.
- 972
- 973 Longley, I., Buessenschuett, C., Clydsdale, L., Cubitt, C., Davis, R., Johnson, M., Marshall, N.,
974 Murray, A., *et al.* 2002. The North West Shelf of Australia—a Woodside perspective. *The sedimentary*
975 *basins of Western Australia*, **3**, 27-88.
- 976
- 977 Mackenzie, G., Thybo, H. & Maguire, P. 2005. Crustal velocity structure across the Main Ethiopian
978 Rift: results from two-dimensional wide-angle seismic modelling. *Geophysical Journal International*,
979 **162**, 994-1006.
- 980

981 MacLeod, S.J., Williams, S.E., Matthews, K.J., Müller, R.D. & Qin, X. 2017. A global review and
982 digital database of large-scale extinct spreading centers. *Geosphere*, **13**, 911-949.

983
984 Maus, S., Barckhausen, U., Berkenbosch, H., Bournas, N., Brozena, J., Childers, V., Dostaler, F.,
985 Fairhead, J., *et al.* 2009. EMAG2: A 2-arc min resolution Earth Magnetic Anomaly Grid compiled
986 from satellite, airborne, and marine magnetic measurements. *Geochemistry, Geophysics, Geosystems*,
987 **10**.

988
989 McDermott, C., Lonergan, L., Collier, J.S., McDermott, K.G. & Bellingham, P. 2018.
990 Characterization of Seaward-Dipping Reflectors Along the South American Atlantic Margin and
991 Implications for Continental Breakup. *Tectonics*, **37**, 3303-3327.

992
993 McDermott, C., Collier, J.S., Lonergan, L., Fruehn, J. & Bellingham, P. 2019. Seismic velocity
994 structure of seaward-dipping reflectors on the South American continental margin. *Earth and
995 Planetary Science Letters*, **521**, 14-24.

996
997 Menard, H. 1969. Elevation and subsidence of oceanic crust. *Earth and Planetary Science Letters*, **6**,
998 275-284.

999
1000 Menzies, M., Klemperer, S., Ebinger, C. & Baker, J. 2002. Characteristics of volcanic rifted margins.
1001 *In: Menzies, M., Klemperer, S., Ebinger, C. & Baker, J. (eds) Volcanic Rifted Margins, Special
1002 Publications*. Geological Society of America, **362**, 1-14.

1003
1004 Meyer, B., Chulliat, A. & Saltus, R. 2017. Derivation and error analysis of the Earth Magnetic
1005 Anomaly Grid at 2 arc min Resolution Version 3 (EMAG2v3). *Geochemistry, Geophysics,
1006 Geosystems*, **18**, 4522-4537.

1007
1008 Mihut, D. & Müller, R.D. 1998. Volcanic margin formation and Mesozoic rift propagators in the
1009 Cuvier Abyssal Plain off Western Australia. *Journal of Geophysical Research*, **103**, 27135-
1010 27127,27149.

1011
1012 Moulin, M., Aslanian, D. & Unternehr, P. 2010. A new starting point for the South and Equatorial
1013 Atlantic Ocean. *Earth-Science Reviews*, **98**, 1-37.

1014
1015 Mutter, J.C., Talwani, M. & Stoffa, P.L. 1982. Origin of seaward-dipping reflectors in oceanic crust
1016 off the Norwegian margin by “subaerial sea-floor spreading”. *Geology*, **10**, 353-357.

1017
1018 Nirrengarten, M., Mohn, G., Kusznir, N., Sapin, F., Despinois, F., Pubellier, M., Chang, S., Larsen,
1019 H., *et al.* 2020. Extension modes and breakup processes of the southeast China-Northwest Palawan
1020 conjugate rifted margins. *Marine and petroleum geology*, **113**, 104123.

1021
1022 Norcliffe, J.R., Paton, D.A., Mortimer, E.J., McCaig, A.M., Nicholls, H., Rodriguez, K., Hodgson, N.
1023 & Van Der Spuy, D. 2018. Laterally Confined Volcanic Successions (LCVS); recording rift-jumps
1024 during the formation of magma-rich margins. *Earth and Planetary Science Letters*, **504**, 53-63.

1025

- 1026 Olierook, H.K., Merle, R.E., Jourdan, F., Sircombe, K., Fraser, G., Timms, N.E., Nelson, G., Dadd,
1027 K.A., *et al.* 2015. Age and geochemistry of magmatism on the oceanic Wallaby Plateau and
1028 implications for the opening of the Indian Ocean. *Geology*, **43**, 971-974.
- 1029
1030 Oosting, A., Leereveld, H., Dickens, G., Henderson, R. & Brinkhuis, H. 2006. Correlation of
1031 Barremian-Aptian (mid-Cretaceous) dinoflagellate cyst assemblages between the Tethyan and Austral
1032 realms. *Cretaceous Research*, **27**, 792-813.
- 1033
1034 Parsons, B. & Sclater, J.G. 1977. An analysis of the variation of ocean floor bathymetry and heat flow
1035 with age. *Journal of Geophysical Research*, **82**, 803-827.
- 1036
1037 Partington, M., Aurisch, K., Clark, W., Newlands, I., Phelps, S., Senyica, P., Siffleet, P. & Walker, T.
1038 2003. The hydrocarbon potential of exploration permits WA-299-P and WA-300-P, Carnarvon Basin:
1039 a case study. *The APPEA Journal*, **43**, 339-361.
- 1040
1041 Paton, D., Pindell, J., McDermott, K., Bellingham, P. & Horn, B. 2017. Evolution of seaward-dipping
1042 reflectors at the onset of oceanic crust formation at volcanic passive margins: Insights from the South
1043 Atlantic. *Geology*, **45**, 439-442.
- 1044
1045 Phipps-Morgan, J. & Chen, Y.J. 1993. The genesis of oceanic crust: Magma injection, hydrothermal
1046 circulation, and crustal flow. *Journal of Geophysical Research: Solid Earth*, **98**, 6283-6297.
- 1047
1048 Plank, T. & Langmuir, C.H. 1998. The chemical composition of subducting sediment and its
1049 consequences for the crust and mantle. *Chemical Geology*, **145**, 325-394.
- 1050
1051 Planke, S. & Eldholm, O. 1994. Seismic response and construction of seaward dipping wedges of
1052 flood basalts: Vøring volcanic margin. *Journal of Geophysical Research: Solid Earth*, **99**, 9263-9278.
- 1053
1054 Planke, S., Symonds, P.A., Alvestad, E. & Skogseid, J. 2000. Seismic volcanostratigraphy of large-
1055 volume basaltic extrusive complexes on rifted margins. *Journal of Geophysical Research: Solid
1056 Earth*, **105**, 19335-19351.
- 1057
1058 Rabinowitz, P.D. & LaBrecque, J. 1979. The Mesozoic South Atlantic Ocean and evolution of its
1059 continental margins. *Journal of Geophysical Research: Solid Earth*, **84**, 5973-6002.
- 1060
1061 Reeve, M.T., Jackson, C.A.L., Bell, R.E., Magee, C. & Bastow, I.D. 2016. The stratigraphic record of
1062 prebreakup geodynamics: Evidence from the Barrow Delta, offshore Northwest Australia. *Tectonics*,
1063 **35**, 1935-1968.
- 1064
1065 Rey, S.S., Planke, S., Symonds, P.A. & Faleide, J.I. 2008. Seismic volcanostratigraphy of the
1066 Gascoyne margin, Western Australia. *Journal of Volcanology and Geothermal Research*, **172**, 112-
1067 131.
- 1068
1069 Robb, M.S., Taylor, B. & Goodliffe, A.M. 2005. Re-examination of the magnetic lineations of the
1070 Gascoyne and Cuvier Abyssal Plains, off NW Australia. *Geophysical Journal International*, **163**, 42-
1071 55.

- 1072
1073 Roberts, D., Backman, J., Morton, A., Murray, J. & Keene, J. 1984. *Evolution of volcanic rifted*
1074 *margins – synthesis of leg-81 results on the West margin of Rockall Plateau.*
- 1075
1076 Robinson, P.T., Thayer, P., Cook, P., McKnight, B. & et al. 1974. *Lithology of Mesozoic and*
1077 *Cenozoic sediments of the eastern Indian Ocean, Leg 27, Deep Sea Drilling Project.*
- 1078
1079 Rudnick, R.L. & Fountain, D.M. 1995. Nature and composition of the continental crust: a lower
1080 crustal perspective. *Reviews of Geophysics*, **33**, 267-309.
- 1081
1082 Sayers, J., Borissova, I., Ramsay, D. & Symonds, P. 2002. *Geological framework of the Wallaby*
1083 *Plateau and adjacent areas.*
- 1084
1085 Scheibnerová, V. 1974. *Aptian–Albian benthonic foraminifera from DSDP Leg 27, Sites 259, 260 and*
1086 *263, Eastern Indian Ocean.*
- 1087
1088 Skogseid, J., Pedersen, T., Eldholm, O. & Larsen, B.T. 1992. Tectonism and magmatism during NE
1089 Atlantic continental break-up: the Voring Margin. *Geological Society, London, Special Publications*,
1090 **68**, 305-320.
- 1091
1092 Skogseid, J., Planke, S., Faleide, J.I., Pedersen, T., Eldholm, O. & Neverdal, F. 2000. NE Atlantic
1093 continental rifting and volcanic margin formation. *In: Nottvedt, A. (ed) Dynamics of the Norwegian*
1094 *Margin*. Geological Society, London, Special Publications, London, **167**, 295-326.
- 1095
1096 Stagg, H., Alcock, M., Bernardel, G., Moore, A., Symonds, P. & Exon, N. 2004. *Geological*
1097 *framework of the outer Exmouth Plateau and adjacent ocean basins*. Geoscience Australia.
- 1098
1099 Stein, C.A. & Stein, S. 1992. A model for the global variation in oceanic depth and heat flow with
1100 lithospheric age. *Nature*, **359**, 123.
- 1101
1102 Stilwell, J., Quilty, P. & Mantle, D. 2012. Paleontology of Early Cretaceous deep-water samples
1103 dredged from the Wallaby Plateau: new perspectives of Gondwana break-up along the Western
1104 Australian margin. *Australian Journal of Earth Sciences*, **59**, 29-49.
- 1105
1106 Sun, S.-S. & McDonough, W.F. 1989. Chemical and isotopic systematics of oceanic basalts:
1107 implications for mantle composition and processes. *In: Saunders, A. & Norry, M. (eds) Magmatism in*
1108 *Ocean Basins*. Geological Society, London, Special Publications, **42**, 313-345.
- 1109
1110 Symonds, P.A., Planke, S., Frey, O. & Skogseid, J. 1998. Volcanic evolution of the Western
1111 Australian Continental Margin and its implications for basin development. *The Sedimentary Basins of*
1112 *Western Australia 2: Proc. of Petroleum Society Australia Symposium, Perth, WA.*
- 1113
1114 Talwani, M. & Eldholm, O. 1973. Boundary between continental and oceanic crust at the margin of
1115 rifted continents. *Nature*, **241**, 325.
- 1116

1117 Tian, X. & Buck, W.R. 2019. Lithospheric thickness of volcanic rifting margins: Constraints from
1118 seaward dipping reflectors. *Journal of Geophysical Research: Solid Earth*, **124**, 3254-3270.

1119
1120 Tischer, M. 2006. *The structure and development of the continent-ocean transition zone of the*
1121 *Exmouth Plateau and Cuvier margin, Northwest Australia: implications for extensional strain*
1122 *partitioning*. PhD, Columbia University.

1123
1124 Tivey, M.A., Johnson, H.P., Fleutelot, C., Hussenoeder, S., Lawrence, R., Waters, C. & Wooding, B.
1125 1998. Direct measurement of magnetic reversal polarity boundaries in a cross-section of oceanic
1126 crust. *Geophysical Research Letters*, **25**, 3631-3634.

1127
1128 Veevers, J. 1986. Breakup of Australia and Antarctica estimated as mid-Cretaceous (95±5 Ma) from
1129 magnetic and seismic data at the continental margin. *Earth and Planetary Science Letters*, **77**, 91-99.

1130
1131 Veevers, J. & Johnstone, M. 1974. Comparative stratigraphy and structure of the western Australian
1132 margin and the adjacent deep ocean floor. *Initial Reports of the Deep Sea Drilling Project*, **27**, 571-
1133 585.

1134
1135 Vine, F.J. 1966. Spreading of the ocean floor: new evidence. *Science*, **154**, 1405-1415.

1136
1137 Vine, F.J. & Matthews, D.H. 1963. Magnetic anomalies over oceanic ridges. *Nature*, **199**, 947-949.

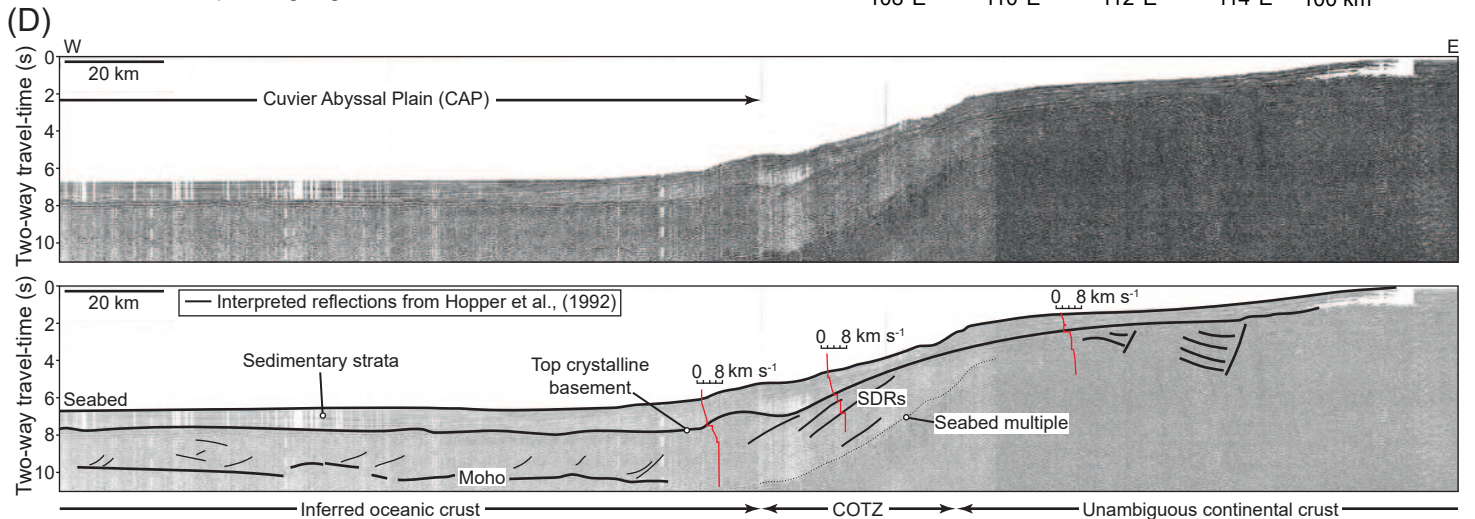
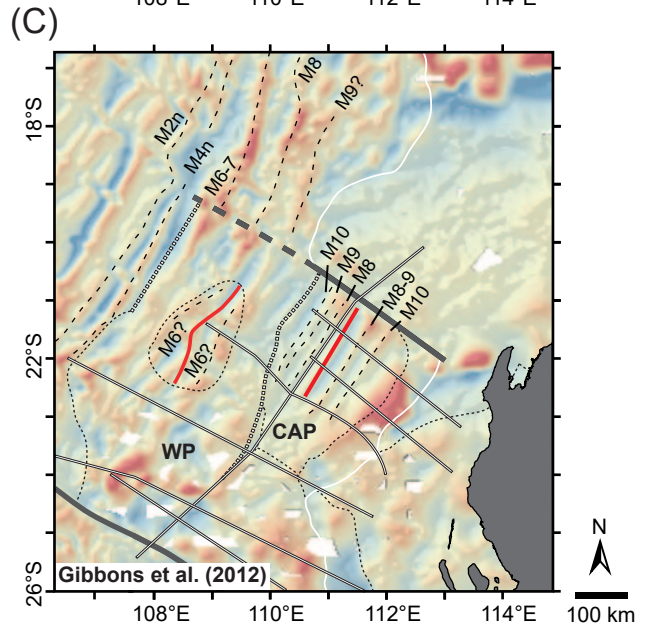
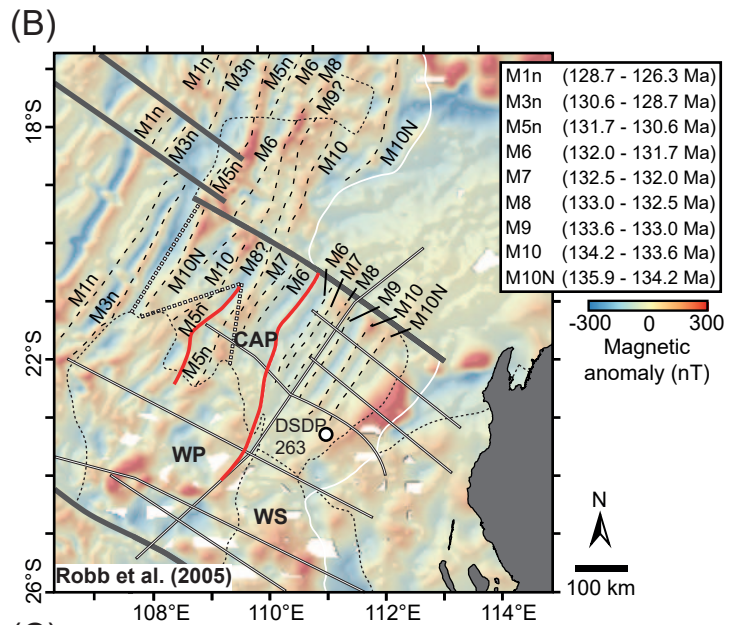
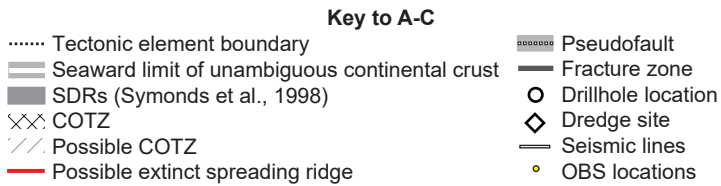
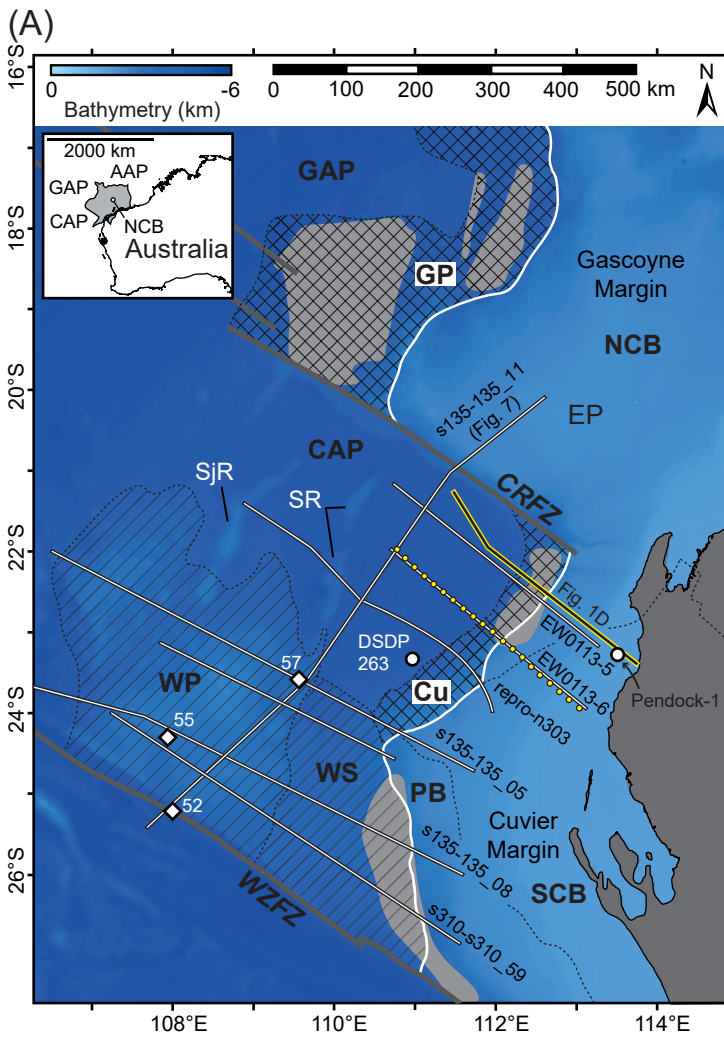
1138
1139 Wiseman, J.F. & Williams, A. 1974. *Palynological investigation of samples from sites 259, 261, and*
1140 *263, Leg 27, Deep Sea Drilling Project*.

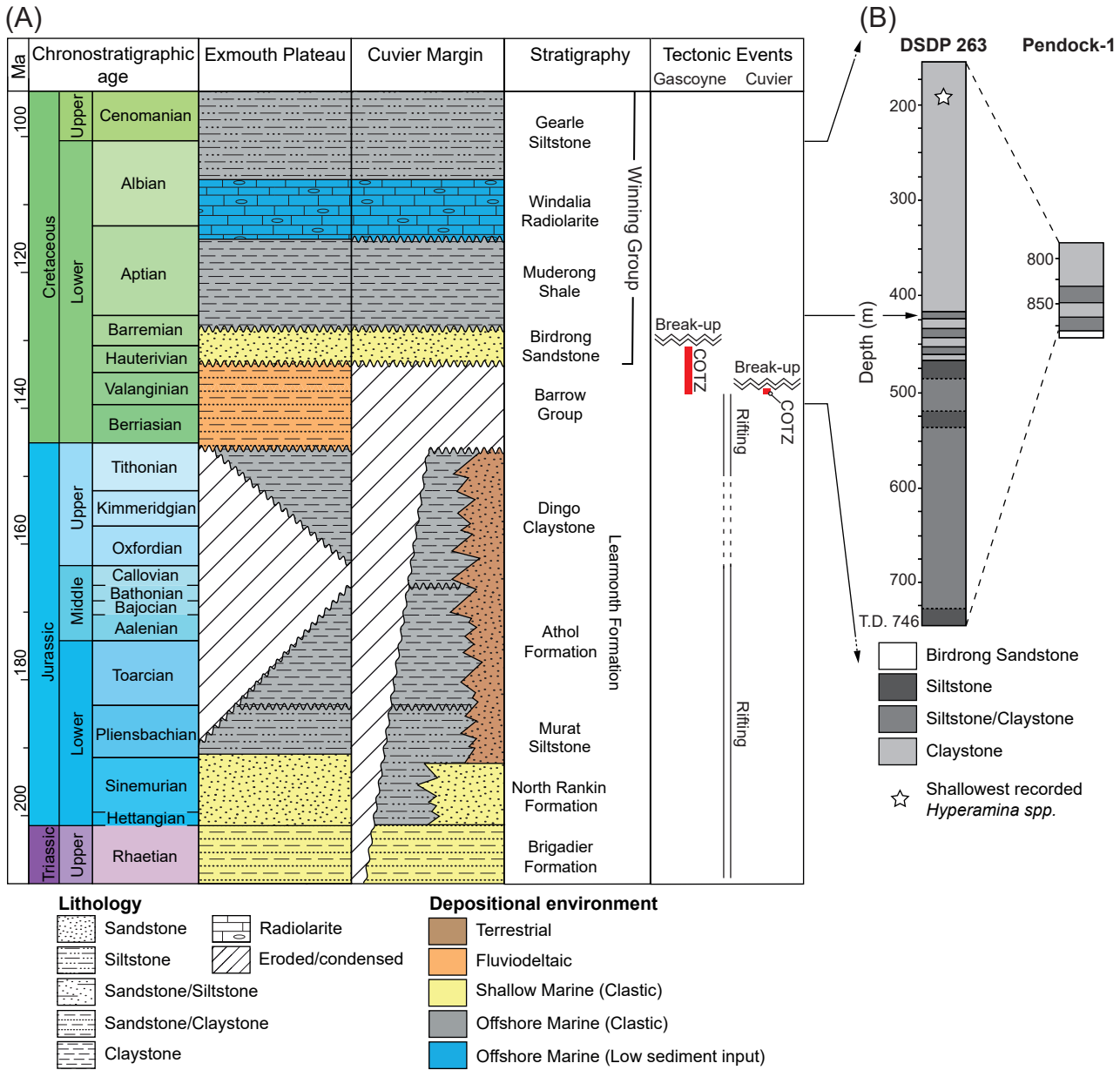
1141
1142
1143
1144
1145
1146
1147
1148
1149
1150
1151
1152
1153

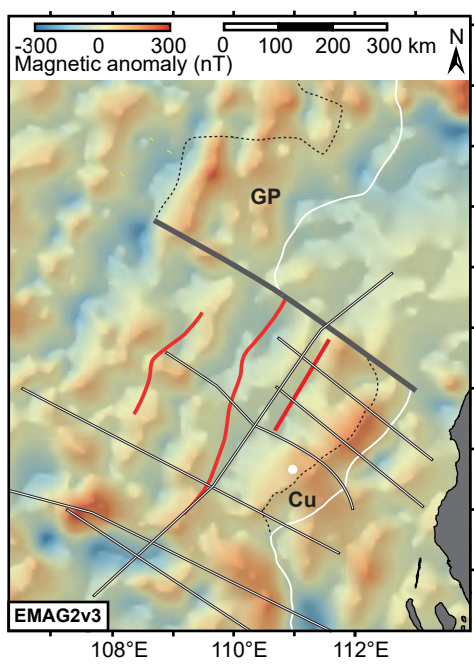
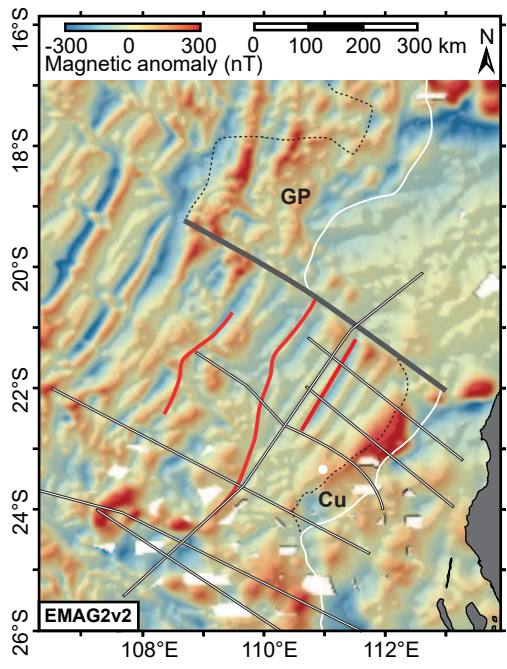
Table 1: Average interval velocities obtained from OBS array

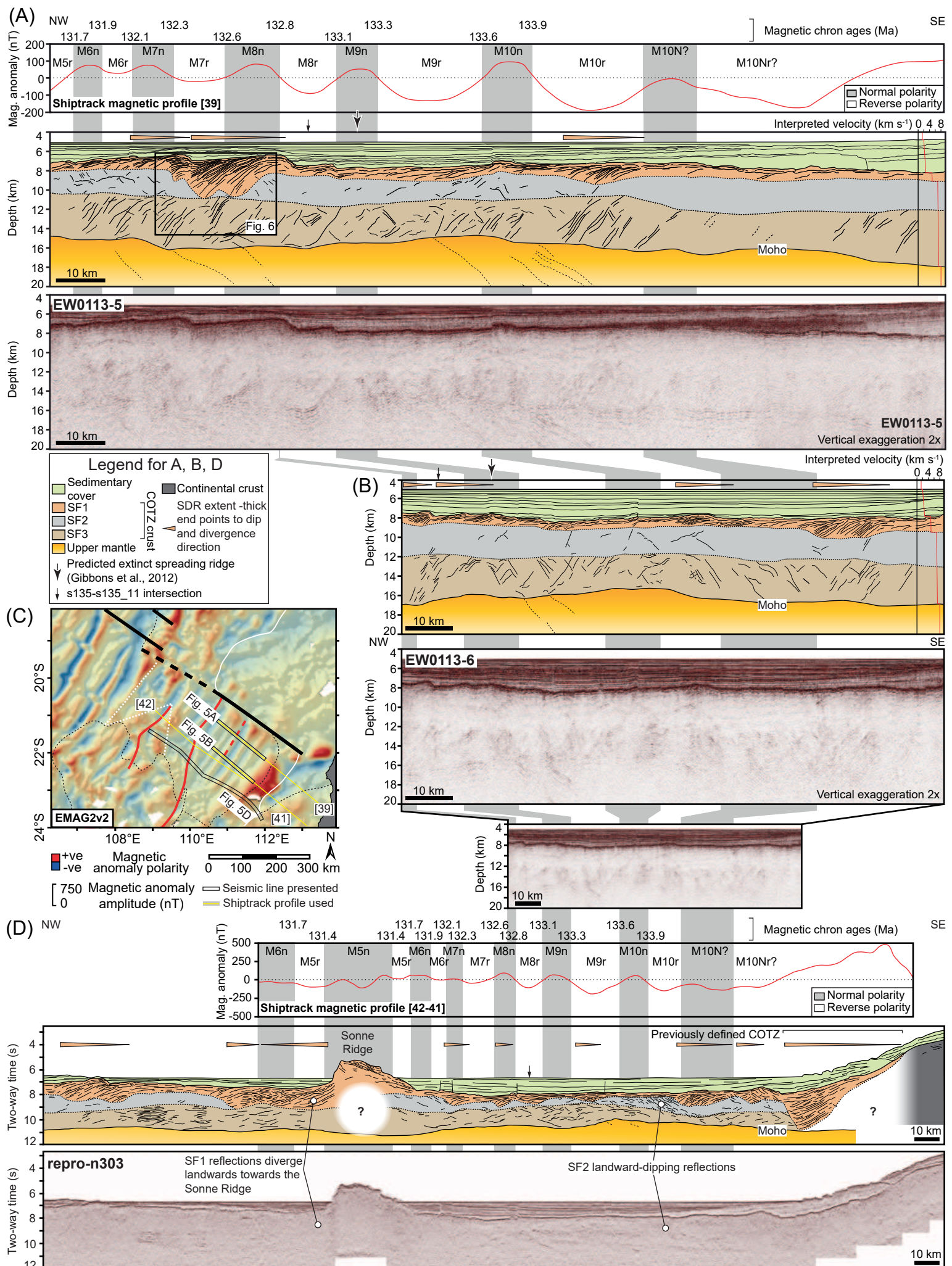
Layer	Seismic velocity (km s ⁻¹)
Water column	1.5
Sedimentary strata	2.0–2.8
Seaward-dipping reflectors (SDRs)	4.9
Sub-SDR crust	6.8–7.2
Upper mantle	8

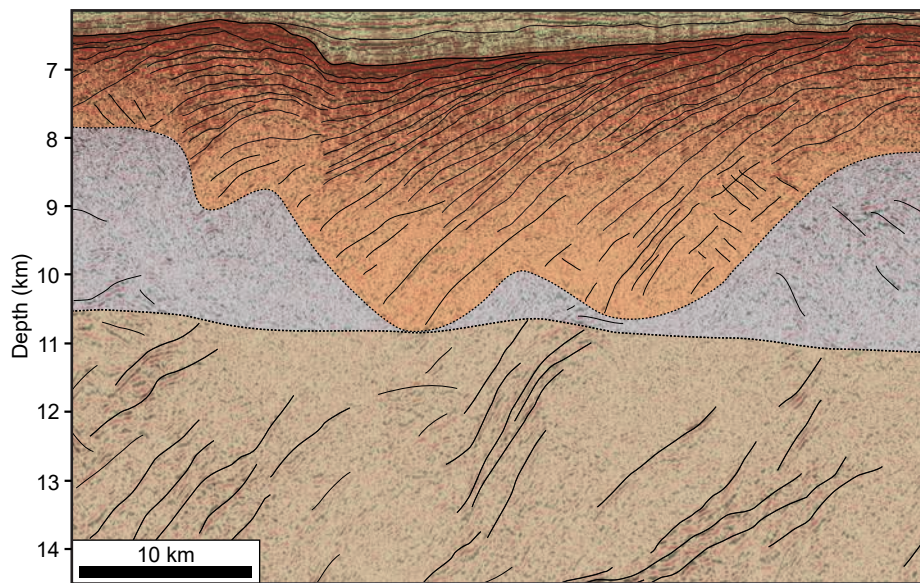
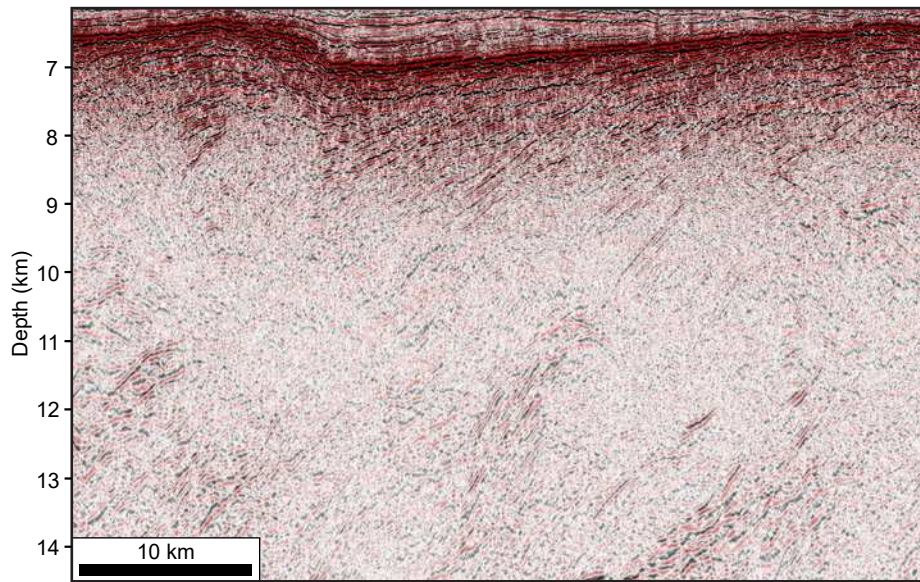
1154

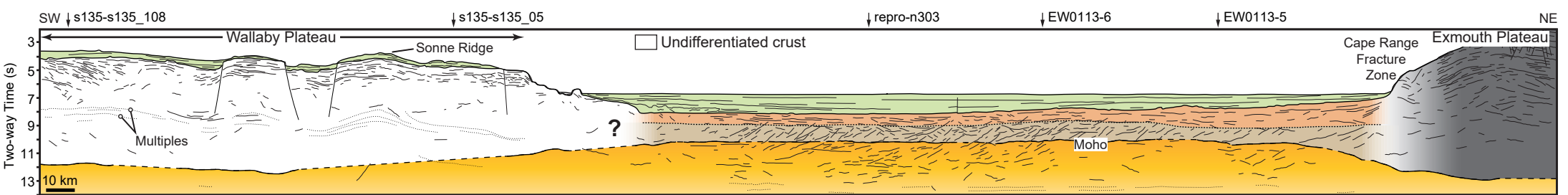


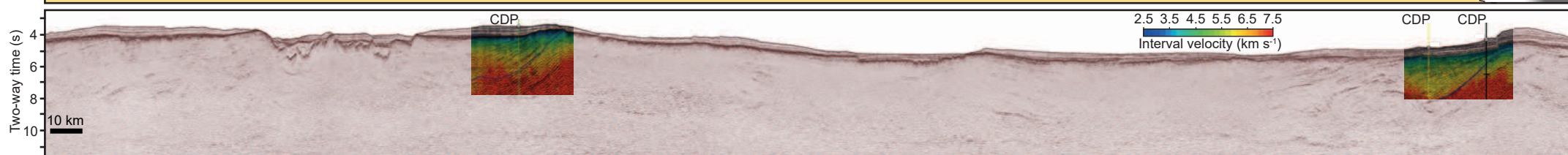
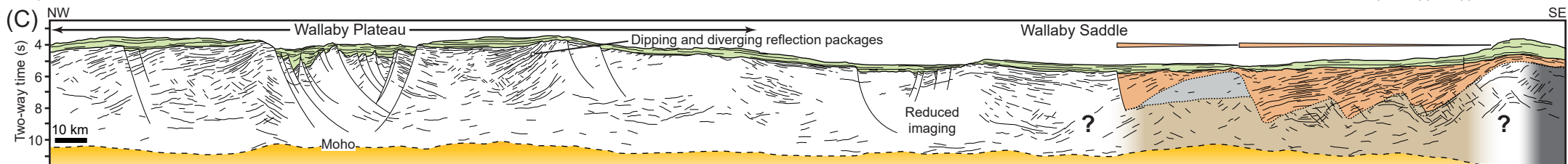
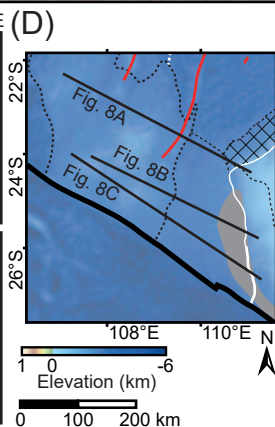
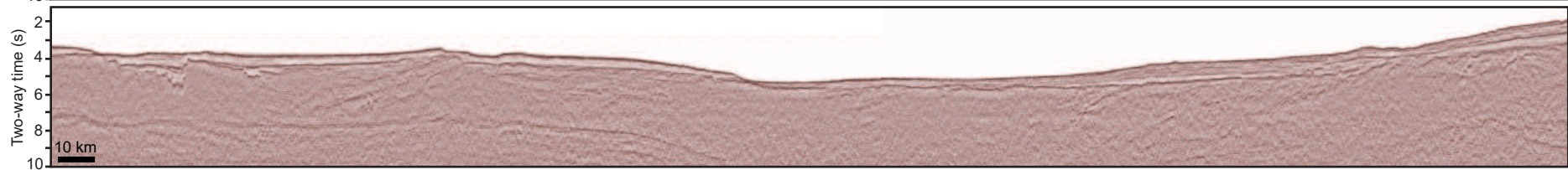
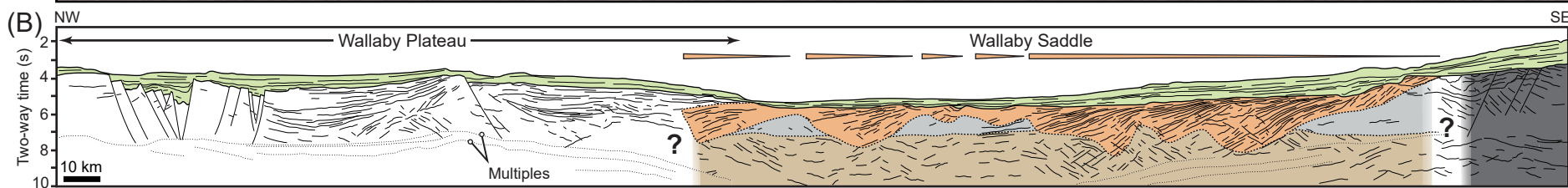
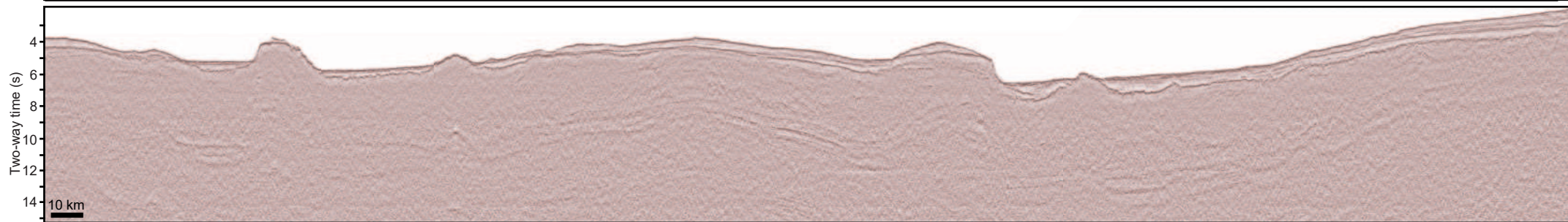
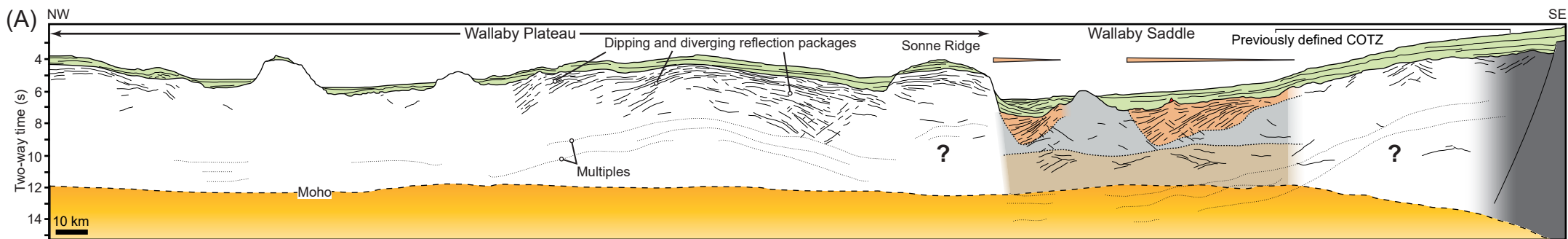


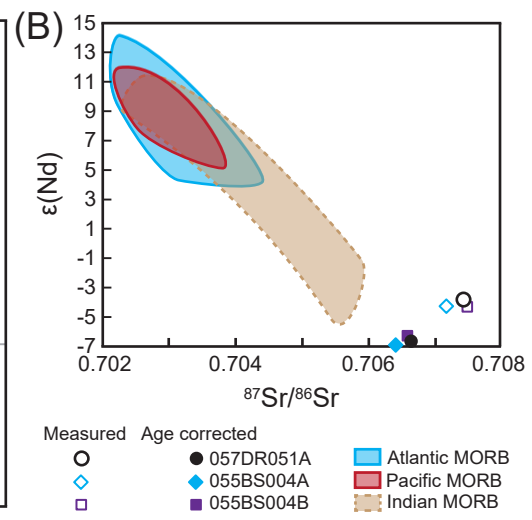
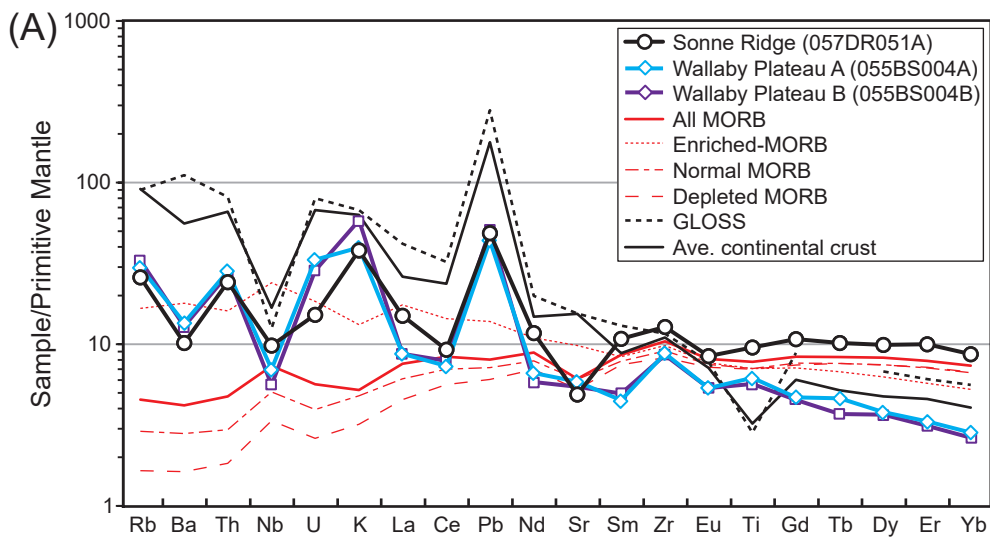




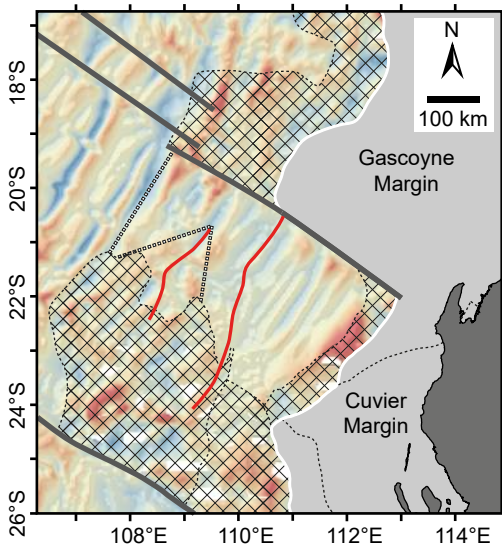




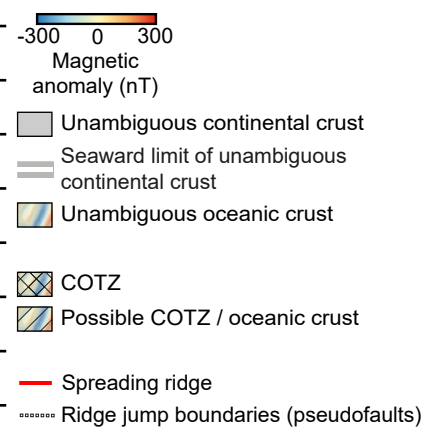
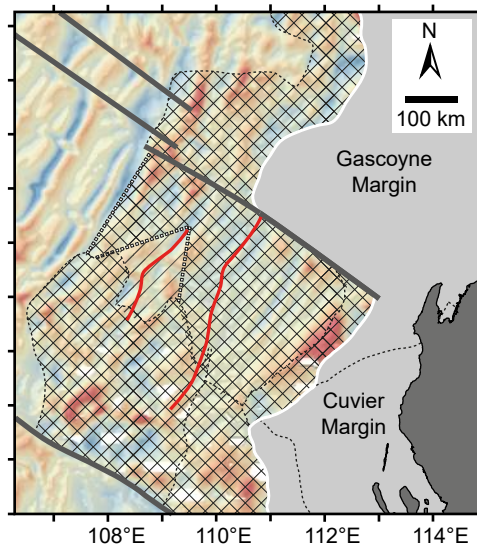




(A) Previous model: CAP = oceanic crust



(B) Proposed alternative: CAP = COTZ



(C)

